GEODYNAMICS & TECTONOPHYSICS

PUBLISHED BY THE INSTITUTE OF THE EARTH'S CRUST
SIBERIAN BRANCH OF RUSSIAN ACADEMY OF SCIENCES

2015 VOLUME 6 ISSUE 3 PAGES 311–344 ISSN 2078-502X

http://dx.doi.org/10.5800/GT-2015-6-3-0184



# METASOMATIC AND MAGMATIC PROCESSES IN THE MANTLE LITHOSPHERE OF THE BIREKTE TERRAIN OF THE SIBERIAN CRATON AND THEIR EFFECT ON THE LITHOSPHERE EVOLUTION

**L. V. Solov'eva[1], T. V. Kalashnikova[2], S. I. Kostrovitsky[2], A. V. Ivanov[1], S. S. Matsuk[3], L. F. Suvorova[2]**

[1] *Institute of the Earth's Crust, Siberian Branch of RAS, Irkutsk, Russia*
[2] *A.P. Vinogradov Institute of Geochemistry, Siberian Branch of RAS, Irkutsk, Russia*
[3] *M.P. Semenenko Institute of Geochemistry, Mineralogy and Ore Formation, National Academy of Sciences of Ukraine, Kiev, Ukraine*

**Abstract:** The area of studies covers the north-eastern part of the Siberian craton (the Birekte terrain), Russia. The influence of metasomatic and magmatic processes on the mantle lithosphere is studied based on results of analyses of phlogopite- and phlogopite-amphibole-containing deep-seated xenoliths from kimberlites of the Kuoika field. In the kimberlitic pipes, deep-seated xenoliths with mantle phlogopite- and phlogopite-amphibole mineralization are developed in two genetically different rock series: magnesian (Mg) pyroxenite-peridotite series (with magnesian composition of rocks and minerals) and phlogopite-ilmenite (Phl-Ilm) hyperbasite series (with ferrous types of rocks and minerals). This paper is focused on issues of petrography and mineralogy of the xenoliths and describes the evidence of metasomatic / magmatic genesis of phlogopite and amphibole. We report here the first data set of $^{40}Ar/^{39}Ar$ age determinations for phlogopite from the rocks of the magnesian pyroxenite-peridotite series and the ferrous Phl-Ilm hyperbasite series.

The Mg series is represented by a continuous transition of rocks from Sp, Sp-Grt, Grt clinopyroxenite and ortopyroxenite to websterite and lherzolite. Many researchers consider it as a layered intrusion in the mantle [*Ukhanov et al., 1988; Solov'eva et al., 1994*]. The mantle metasomatic phlogopite and amphibole are revealed in all petrographic types of the rocks in this series and compose transverse veins and irregular patchs at grain boundaries of primary minerals. At contacts of xenolith and its host kimberlite, grains of phlogopite and amphibole are often cut off, which gives an evidence of the development of metasomatic phlogopite-amphibole mineralization in the rocks before its' entraiment into the kimberlite. In the xenoliths with exsolution pyroxene megacrystalls, comprising parallel plates of clino- and orthopyroxene ± garnet ± spinel (former high-temperature pigeonite [*Solov'eva et al., 1994*]), the metasomatic phlogopite-amphibole aggregate mainly replace laminar intergrowths of one of pyroxenes and garnet and also develops in the re-crystallized fine-grained rock matrix. This suggests a considerable period of time between the crystallization of rocks of the pyroxenite-peridotite series and the development of phlogopite-amphibole metasomatism.

The Phl-Ilm hyperbasites comprise a complex association of parageneses represented by garnet- and garnetless pyroxenites, websterites, olivine websterites, orthopyroxenites, lherzolites and olivinites. A specific feature of this series is high contents of K, Ti and Fe in the rocks and minerals. The content of phlogopite is widely variable, from a few percent to 40–80 %. The content of ilmenite ranges from a few percent to 15 %, rarely to 30–40 %. Mica and ilmenite contents sharply decrease in garnetized xenolithes, where these two minerals, as soon as olivine and pyroxenes are replaced by garnet.

Euhedral, subhedral, sideronitic and porphyraceous structures in garnetless xenoliths suggest the primary magmatic genesis of the rocks. In the series of Phl-Ilm hyperbasites, a special type of parageneses is represented by strongly deformed phlogopite-amphibole rocks with newly-formed chromite and relict resorbed ilmenite and clinopyroxene. Phl-Ilm rock series is also characterized by a variety of autometasomatic and metasomatic reaction structures. Garnet and phlogopite develop nearly simultaneously at the sub-solidus stage: garnet develops due to cooling of the primary magmatic rocks, and phlogopite develops under the influence of residual rich in potassium and volatiles fluids – melts. Phlogopite in the rocks of the Phl-Ilm series form porphyraceous plates, late intergranular xenomorphic grains, porphyroblasts of the solidus stage and strongly deformed irregular plates in the phlogopite-amphibole rocks. Amphibole occurs in garnetless parageneses and deformed phlogopite-amphibole rocks in amounts of a few percent and up to 40–50%, respectively. Petrographically, the differentiated series of phlogopite-ilmenite hyperbasites belongs to mantle magmatites, except for younger deformed phlogopite-amphibole rocks from zones of deep faults.

Unlike corresponding minerals in the Mg pyroxenite-peridotite series, minerals from the Phl-Ilm hyperbasites are characterized by lower magnesium index (Mg#), considerably higher contents of $TiO_2$ and FeO, and lower contents of $Cr_2O_3$ (Table). In diagrams Mg# – $TiO_2$ and Mg# – $Cr_2O_3$, metasomatic phlogopite points from Mg series rocks are significantly distant from points of mica from the phlogopite-ilmenite parageneses (Fig. 24). In the parageneses of the Mg pyroxenite-peridotite series, phlogopite plates have homogenous compositions in contrast to zonal phlogopite in the Phl-Ilm hyperbasites. In Phl-Amph metasomatites of the Mg series, amphibole is represented by typical pargasite, and its chemical composition is sharply different from that of K-richterite from the deformed phlogopite-amphibole rocks of the series of the Phl-Ilm hyperbasites (Table).

The $^{40}Ar/^{39}Ar$ age in the range from 1640 to 1800 Ma (Fig. 25) is determined for phlogopite from the metasomatic phlogopite-amphibole veinlets and intergranular reaction patches in the garnet olivine websterite of the Mg series. For mica from the garnetless Phl-Ilm websterites, ages are 869 and 851 Ma (Fig. 25). Mica from the garnet-containing Phl-Ilm lherzolites is much younger (608 and 495 Ma). The age of mica from the deformed phlogopite-amphibole rock is 167 Ma, which is close to the age of kimberlites of the Kuoika field.

Metasomatic phlogopite (1640–1800 Ma) originated somewhat later than the Birekte terrain accretion to the Siberian craton (1.8–1.9 Ga) [*Rosen*, *2003*], and its age determination may be explained by a partial loss of $^{40}Ar$ in the analysed medium. This age is also close to the late episode when the crust was formed in the Birekte block 1.8–2.1 Ga ago [*Nasdala et al*., *2014*], and corresponds to the time when radiogenic osmium was supplied into the mantle lithosphere from the subduction zone (1.7–2.2 Ga, according to [*Pernet et al*., *2015*]). In analyses of minerals in the pyroxenite-peridotite series from the Obnazhennaya pipe, data on the oxygen isotope geochemistry give evidence of an ancient subduction component (Fig. 26). It can be thus assumed that in the mantle lithosphere of the Birekte terrain, phlogopite-amphibole metasomatism took place due to fluids-melts ascending from the subduction zone about 1.8 Ga ago and correlates to the accretion of this block to the Siberian craton. The complex magmatic series of Phl-Ilm rocks formed later than the Mg pyroxenite-peridotite series. The more ancient ages of phlogopite (869–851 Ma) from Phl-Ilm hyperbasites are somewhat higher than the most ancient dating of alkaline ultrabasic-carbonatite Tomtor massif (800 Ga, according to [*Entin et al*., *1990*]) and the time when the breakup of Rodinia began (825 Ga, according to [*Li et al*., *2008*]). The difference may be explained by an advance occurrence of high-potassium, titanian, ferrous magmatites in the mantle lithosphere of the Birekte block as compared to their appearance on the surface. Phlogopite from xenoliths with subsolidus garnetization is significantly younger in age (500–600 Ma), may be, due to a loss of radiogenic argon caused by mica replacement. $H_2O$, K, Ba, F and Cl were abundantly released during the replacement and supplied into the upper layers of the crust and mantle. The mantle high-potassium and high titanian Phl-Ilm series seems comagmatic with the surficial potassium ultramafites and mafites of the Siberian Platform and associated with the earlier episode of the Rodinia breakup.

**Key words:** Siberian craton, Birekte terrain, lithosphere mantle, mantle xenolith, magmatism, mantle metasomatism, magnesian pyroxenite-peridotite series, ferrous Phl-Ilm hyperbasite series.

**Recommended by** E.V. Sklyarov

**For citation:** *Solov'eva L.V., Kalashnikova T.V., Kostrovitsky S.I., Ivanov A.V., Matsuk S.S., Suvorova L.F.* 2015. Metasomatic and magmatic processes in the mantle lithosphere of the Birekte terrain of the Siberian craton and their effect on the lithosphere evolution. *Geodynamics & Tectonophysics* 6 (3), 311–344. doi: 10.5800/GT-2015-6-3-0184.

# МЕТАСОМАТИЧЕСКИЕ И МАГМАТИЧЕСКИЕ ПРОЦЕССЫ В МАНТИЙНОЙ ЛИТОСФЕРЕ БИРЕКТИНСКОГО ТЕРРЕЙНА СИБИРСКОГО КРАТОНА И ИХ ВЛИЯНИЕ НА ЭВОЛЮЦИЮ ЛИТОСФЕРЫ

**Л. В. Соловьева[1], Т. В. Калашникова[2], С. И. Костровицкий[2], А. В. Иванов[1], С. С. Мацюк[3], Л. Ф. Суворова[2]**

[1] *Институт земной коры СО РАН, Иркутск, Россия*
[2] *Институт геохимии им. А.П. Виноградова СО РАН, Иркутск, Россия*
[3] *Институт геохимии, минералогии и рудообразования им. М.П. Семененко НАН Украины, Киев, Украина*

**Аннотация: Введение.** Влияние процессов мантийного метасоматизма и магматизма на эволюцию литосферной мантии в северо-восточном Биректинском террейне Сибирского кратона рассмотрено на примере флогопит- и флогопит-амфиболсодержащих глубинных ксенолитов из кимберлитов Куойкского поля (рис. 1).

Глубинные ксенолиты с мантийной флогопитовой и флогопит-амфиболовой минерализацией в кимберлитовых трубках поля развиты в двух генетически разных сериях пород: магнезиальной (Mg) пироксенит-перидотитовой (с магнезиальным составом пород и минералов) и в серии флогопит- ильменитовых (Phl-Ilm) гипербазитов (с железистым типом пород и минералов). В настоящей работе уделяется большое внимание петрографии и минералогии ксенолитов с мантийной флогопитовой и флогопит-амфиболовой минерализацией, и приводятся новые данные по $^{40}Ar/^{39}Ar$ возрасту флогопита.

**Методы исследований.** Флогопит- и флогопит-амфиболсодержащие парагенезисы ксенолитов были детально изучены в образцах и шлифах. Зерна минералов были проанализированы на содержания главных оксидов на рентгеновском электронно-зондовом микроанализаторе JXA-8200 в Институте геохимии им. А.П. Виноградова СО РАН (г. Иркутск). Анализ изотопного состава кислорода в гранате выполнен в аналитическом центре ДВГИ ДВО РАН (г. Владивосток) на масс-спектрометре Finnigan MAT 252, [*Ignatiev, Velivetskaya, 2004*]. Определение возраста флогопита $^{40}Ar/^{39}Ar$ методом произведено в Институте земной коры СО РАН (г. Иркутск) с использованием мультиколлекторного масс-спектрометра Argus VI.

**Петрография и минералогия.** Магнезиальная (Mg) серия представлена непрерывным переходом пород от Sp, Sp-Grt, Grt клинопироксенитов, ортопироксенитов к вебстеритам, оливиновым вебстеритам и лерцолитам и рассматривается рядом исследователей как расслоенная интрузия в мантии [*Ukhanov et al., 1988; Solov'eva et al., 1994*]. Мантийная метасоматическая флогопит-амфиболовая минерализация проявлена во всех петрографических типах пород серии и развита в виде секущих прожилков и неправильных участков по границам зерен первичных минералов (рис. 4, 5). В ксенолитах с мегакристаллами пироксенов, состоящих из параллельных пластинок клино- и ортопироксена ± граната ± шпинели (структуры распада высокотемпературного пижонита [*Solov'eva et al., 1994*]), метасоматический флогопит-амфиболовый агрегат развивается преимущественно по пластинчатым вросткам одного из пироксенов и граната и в перекристаллизованной мелкозернистой матрице пород. Это указывает на значительный интервал времени между кристаллизацией пород пироксенит-перидотитовой серии и развитием флогопит-амфиболового метасоматизма.

Phl-Ilm гипербазиты также образуют сложную ассоциацию парагенезисов, представленных Phl-Ilm гранатовыми и безгранатовыми пироксенитами, вебстеритами, оливиновыми вебстеритами, ортопироксенитами, лерцолитами и оливинитами. Характерной особенностью серии являются высокие содержания K, Ti, Fe в породах и минералах. Содержание флогопита в породах широко варьируется – от первых процентов до 40–80 %, ильменита – от первых до 15 %, реже до 30–40 %. Количество слюды и ильменита резко уменьшается в гранатизированных ксенолитах, в которых гранат интенсивно замещает эти минералы, а также первичные силикаты. Панидиоморфнозернистые, гипидиоморфнозернистые, сидеронитовые и порфировидные структуры в негранатизированных ксенолитах указывают на первичный магматический генезис пород. Для пород серии характерно также разнообразие автометасоматических и метасоматических структур. Гранат и флогопит развиваются на субсолидусном этапе близко одновременно: первый за счет охлаждения первичных магматических пород (рис. 11, 12, 14), а второй при воздействии на них остаточных флюидов-расплавов, обогащенных калием и летучими (рис. 8). Особый тип парагенезисов в серии Phl-Ilm гипербазитов представляют сильно деформированные флогопит-амфиболовые породы с новообразованным хромитом и с реликтовыми резорбированными ильменитом и клинопироксеном (рис. 21–23). Дифференцированная серия флогопит-ильменитовых гипербазитов по петрографическим признакам относится к мантийным магматитам, за исключением более поздних деформированных флогопит-амфиболовых пород из зон глубинных разломов.

В отличие от соответствующих минералов Mg пироксенит-перидотитовой серии, минералы из Phl-Ilm гипербазитов имеют значительно меньшую магнезиальность (Mg#) и содержат существенно больше $TiO_2$, FeO и меньше $Cr_2O_3$ (таблица). Точки метасоматических флогопитов из пород Mg серии на диаграммах Mg# – $TiO_2$ и Mg# – $Cr_2O_3$ существенно отделены от поля точек слюд из флогопит-ильменитовых парагенезисов (рис. 24). Амфибол, представленный в Phl-Amph метасоматитах Mg серии типичным паргаситом по химическому составу резко отличается от K-рихтерита из деформированных флогопит-амфиболовых пород серии Phl-Ilm гипербазитов (таблица).

**$^{40}Ar/^{39}Ar$ датирование слюды.** $^{40}Ar/^{39}Ar$ возраст флогопита из метасоматических флогопит-амфиболовых прожилков и межзерновых реакционных обособлений в гранатовом оливиновом вебстерите Mg серии варьируется в пределах 1640–1800 млн лет (рис. 25). Слюды из негранатизированных Phl-Ilm вебстеритов показали возраст 869 и 851 млн лет (рис. 25). В гранатизированных Phl-Ilm лерцолитах возраст слюд значительно меньше (608 и 495 млн лет). Слюда из деформированной флогопит-амфиболовой породы показала возраст 167 млн лет, близкий возрасту кимберлитов Куойкского поля.

**Дискуссия и результаты.** Возраст метасоматического флогопита (1640–1800 млн лет) несколько ниже возраста присоединения Биректинского террейна к Сибирскому кратону (1.8–1.9 млн лет [*Rosen, 2003*]), что, возможно, объясняется частичной потерей $^{40}Ar$ в анализируемой слюде. С другой стороны, это значение близко интервалу позднего эпизода формирования коры в Биректинском блоке 1.8–2.1 млрд лет [*Nasdala et al., 2014*] и соответствует времени привноса радиогенного осмия в мантийную литосферу из зоны субдукции (1.7–2.2 лет [*Pernet-Fisher et al., 2015*]). Геохимия изотопов кислорода в породах перидотит-пироксенитовой серии из трубки Обнаженная также свидетельствует о присутствии в них древней субдукционной компоненты (рис. 26). Это позволяет предположить, что мантийный флогопит-амфиболовый метасоматизм в литосферной мантии Биректинского террейна осуществлялся флюидами – расплавами, поступавшими из зоны субдукции примерно 1.8 млрд лет назад, и соответствует эпизоду присоединения этого блока к Сибирскому кратону.

Сложная магматическая серия Phl-Ilm пород является более поздней по сравнению с Mg пироксенит-перидотитовой серией. Древний возраст флогопита (869–851 млн лет) из Phl-Ilm гипербазитов несколько превышает наиболее древние датировки щелочного ультраосновного – карбонатитового Томторского массива (800 млн лет [*Entin et al., 1990*]) и время начала распада суперконтинента Родиния (825 млн лет [*Li et al., 2008*]). Эта разница может быть объяснена опережающим проявлением высококалиевых, титанистых, желе-

зистых магматитов в мантийной литосфере Биректинского блока по сравнению с их проявлением на поверхности. Флогопит из ксенолитов с субсолидусной гранатизацией показывает существенно меньшие значения возраста (500–600 млн лет), вероятно, из-за потери радиогенного аргона при замещении слюды. Этот процесс высвобождал большое количество $H_2O$, K, Ba, F и Cl, поступавших в верхние горизонты коры и мантии. Мантийная высококалиевая и высокотитанистая Phl-Ilm серия, по-видимому, комагматична поверхностным калиевым ультрамафитам и мафитам на Сибирской платформе и связана с ранним эпизодом раскола суперконтинента Родиния.

**Главные выводы.** 1. Рассмотренные флогопитсодержащие серии ксенолитов из кимберлитовых трубок Куойкского поля принадлежат к разным генетическим образованиям и к разным этапам эволюции литосферной мантии Биректинского террейна. 2. Phl-Amph метасоматизм развивается по породам сложной магнезиальной пироксенит-перидотитовой серии ксенолитов, имеет геохимические черты зоны субдукции и маркирует этап, связанный с присоединением Биректинского континентального блока к Сибирскому кратону ~1.8–1.9 млрд лет. 3. Сложная железистая серия Phl-Ilm гипербазитов относится к типичным мантийным калиевым ультраосновным – основным магматитам. Начало формирования магматической серии Phl-Ilm гипербазитов в мантийной литосфере Биректинского террейна (~869–851 млн лет), возможно, соответствует самому раннему этапу распада суперконтинента Родиния.

**Ключевые слова:** Сибирский кратон, Биректинский террейн, литосферная мантия, мантийные ксенолиты, магматизм, мантийный метасоматизм, магнезиальная пироксенит-перидотитовая серия, серия железистых флогопит-ильменитовых гипербазитов.

## 1. Introduction

The Birekte terrain is located in the north-eastern part of the Siberian craton. The geotectonic regional partition suggest that it was formed not later than 2.4 Ga ago (Fig. 1) [*Rosen*, *2003*]. The composition and structure of the mantle lithosphere of this block were mainly discovered by studies of deep-seated xenoliths from the Upper Jurassic–Lower Cretaceous Kuoika kimberlite field [*Ukhanov et al*., *1988; Solov'eva et al., 1994; Howarth et al., 2014*]. It has been noted in many publications that the mantle lithosphere in the north-eastern part of the Siberian craton is significantly different from that of its central part in terms of both thickness and composition [*Pokhilenko et al*., *1999*].

Our study is focused on deep-seated xenoliths with mantle phlogopite- and phlogopite-amphibole mineralization which are found in kimberlite pipes of the Kuoika field (Obnazhennaya, Slyudyanka, Pyatnitsa pipes). The occurrence of primary phlogopite and amphibole in deep-seated xenoliths is generally viewed as a result of different-aged processes of mantle metasomatism [*Menzies, Hawkesworth*, *1987*]. It is remarkable that primary phlogopite in deep-seated xenoliths may be of magmatic genesis [*Solovieva et al*., *1997*].

According to [*Garanin et al., 1985; Ukhanov et al., 1988*], phlogopite- and phlogopite-amphibole mineralization was discovered in two series of deep-seated xenoliths from the Obnazhennaya pipe (Kuoika field), specifically the Mg pyroxenite-peridotite series and the series of Phl-Ilm hyperbasites with a higher Fe content. Nevertheless, phlogopite- and phlogopite-amphibole mantle parageneses remain poorly studied in terms of both composition and time of their occurrence in the mantle lithosphere in the north-eastern block of the Siberian craton. This paper is focused on issues of petrography and mineralogy of the xenoliths and the evidences of metasomatic/magmatic genesis of mantle phlogopite and amphibole. We report here the first data of $^{40}Ar/^{39}Ar$ age determinations for phlogopite from the rocks of the magnesian pyroxenite-peridotite series and the ferrous Phl-Ilm hyperbasite series. Results of our studies reveal the genesis of phlogopite- and phlogopite-amphibole mantle mineralization and its relationships with evolution stages of the mantle lithosphere in the north-eastern block of the Siberian craton.

## 2. Research methods

Detailed studies of phlogopite and phlogopite- amphibole xenoliths are conducted using rock samples and thin sections. The mantle genesis of mica and amphibole is determined by a number of signs, such as the development of these minerals in a xenolith regardless of a distance to kimberlite, cut-off of phlogopite plates and amphibole grains by the xenolith contact, the composition of phlogopite etc. The fine-grained mica filling the cracks coming from the kimberlite into the xenolith is not considered as pre-kimberlite/mantle one. Grains of minerals are analysed for the main oxides. The analyses were taken using Electron Probe Microanalyzer JXA-8200 at the Vinogradov Institute of Geochemistry, Irkutsk. The isotopes of oxigen were analysed for garnet. We use results of analyses conducted at the Analytical Centre of the Far East Geological Institute, Far East Branch of RAS, using the fluorination $BrF_5$ method

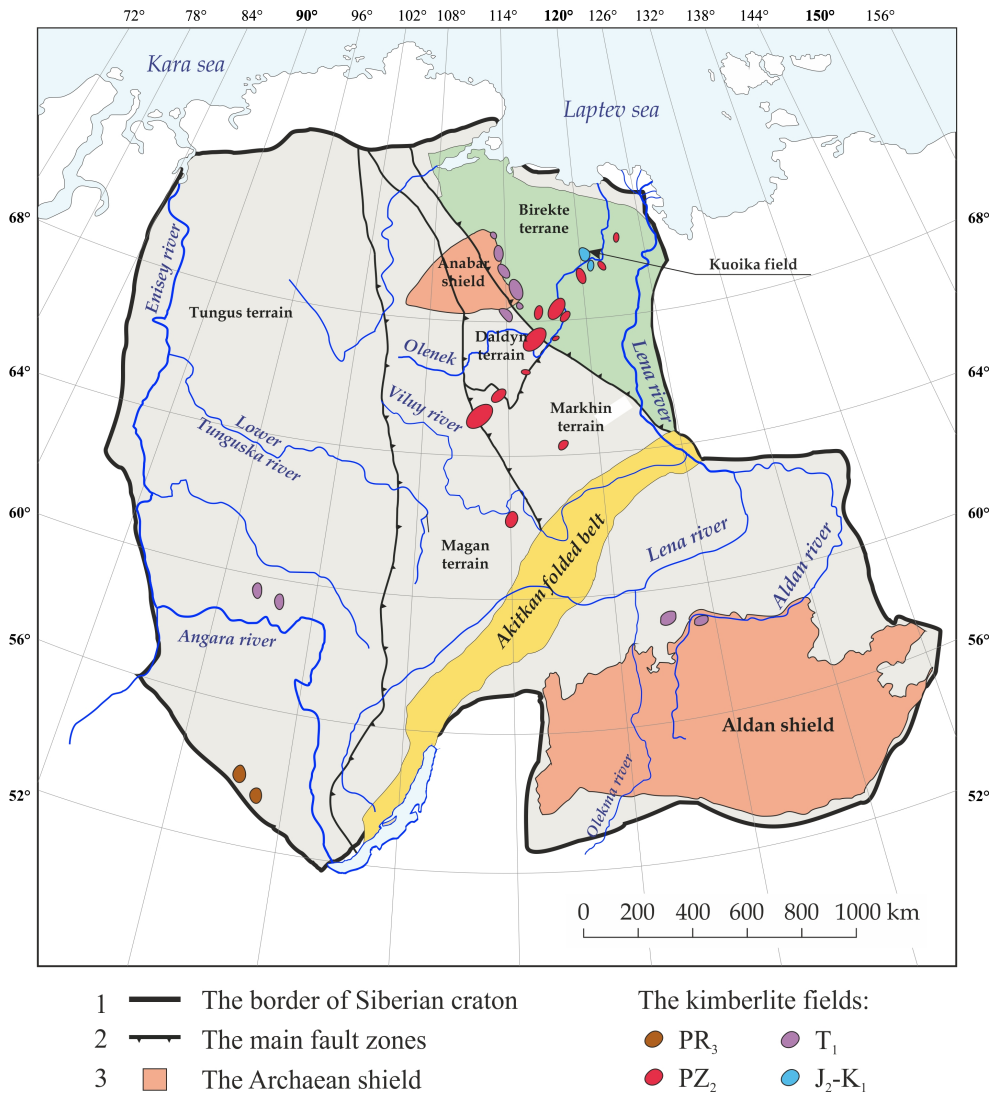


**Fig. 1.** Schematic map of ancient terrains and kimberlitic fields in the Siberian craton with the authors' modification.

The legend is given in the figure. The craton and the kimberlitic fields are contoured according to [*Khar'kiv et al., 1998*], terrains of the Siberian craton according to [*Rosen, 2003*], and the Anabar crystalline shield according to [*Parfenov, Kuzmin, 2001*].

**Рис. 1.** Схема расположения древних террейнов и кимберлитовых полей на Сибирском кратоне с некоторыми изменениями авторов статьи.

Условные обозначения приведены на рисунке. Контуры кратона и кимберлитовые поля нанесены по [*Khar'kiv et al., 1998*]; террейны Сибирского кратона – по [*Rosen, 2003*]; Анабарский кристаллический щит – по [*Parfenov, Kuzmin, 2001*].

[*Ignatiev, Velivetskaya, 2004*]. The weight of mineral fractions for analysis ranges from 1 to 2 mg, precision of the method (1σ) amounts to 0.1 ‰ (n=5). Measurements ($\delta^{18}O$) were conducted with a Finnigan MAT 252 isotope mass spectrometer (IRMS). The repeatability of measurements $\delta^{18}O$ for samples amounts to 0.1 ‰. Dating of phlogopites by $^{40}Ar/^{39}Ar$ method was performed at the Institute of the Earth's Crust, SB RAS; an Argus VI multi-collector mass spectrometer and a high-vacuum oven (dual vacuum, heating above 1700 °C) were used. Mica samples (15–30 mg) were wrapped in an aluminium foil and put into a glass ampoule together with BERN4M standards (assumed age of 18.885±0.097 Ma). The glass ampoule was irradiated in a VVR-K nuclear reactor in Tomsk. Radiation parameters were similar to those reported in [*Travin et al., 2009*].

## 3. Petrography and mineralogy

### 3.1. Phlogopite-amphibole parageneses in the magnesian pyroxenite-peridotite series of the xenoliths

*The Mg pyroxenite-peridotite series of the xenoliths* is represented by a continuous transition of rocks from

Sp, Sp-Grt, Grt clinopyroxenites and ortopyroxenites to Sp, Sp-Grt, Grt websterites, olivine websterites and lherzolites [*Ukhanov et al., 1988*; *Solov'eva et al., 1994*]. The mantle metasomatic phlogopite and amphibole are revealed in all the petrographic types of the rocks in nearly every twentieth xenoliths and typically are composed of transverse veins and veinlet aggregates at grain boundaries of primary minerals. In metasomatic area amphibole predominates. At contacts of xenolith and host kimberlite, grains of phlogopite and amphibole are often cut off, which gives an evidence of the development of metasomatic phlogopite-amphibole mineralization before xenolith entrainment by the kimberlite. In the exsolution pyroxene megacrystalls (former high-temperature pigeonite [*Solov'eva et al., 1994*]), comprising parallel plates of clino- and orthopyroxene ± garnet ± spinel, the metasomatic phlogopite-amphibole aggregate mainly replace laminar intergrowths of one of pyroxenes and garnet (Fig. 2). The abundant development of metasomatic amphibole is observed from the contact with cutting phlogopite-amphibole veinlets (Fig. 3–5). Grains of olivine, garnet and clinopyroxene are intensively resorbed at the boundaries with the veinlets. Small amphibole grains are developed from the veinlet into the grains of clinopyroxene (Fig. 3, *B*). In veinlet selvages, clinopyroxene remains as small irregular relics (Fig. 3, *C*). Garnet is replaced by phlogopite at the contact with the phlogopite infill of the veinlets (Fig. 4, *A*, *B*). In the phlogopite-amphibole parts of the veinlets, the texture is close to magmatic euhedral one (Fig. 4, *C*). The grains of pyroxene are filled by small crystals of metasomatic amphibole (Fig. 5, *A*–*D*) which commonly have one or two crystallographic direction.

The undoubted metasomatic character of the phlogopite-amphibole mineralization in the xenoliths of the magnesian pyroxenite-peridotite series and its development before xenoliths entrainment into the kimberlite melt suggest that this process is related to intensive metasomatism of the mantle lithosphere in the north-eastern part of the Siberian craton.

### 3.2. Phlogopite and phlogopite-amphibole parageneses in xenoliths of the ferrous Phl-Ilm series of hyperbasites

The Phl-Ilm hyperbasites comprise a complex association of parageneses represented by garnet- and garnetless pyroxenites, websterites, olivine websterites, orthopyroxenites, lherzolites and olivinites. High contents of K, Ti and Fe in the rocks and minerals are typical of this series [*Garanin et al., 1985; Ukhanov et al., 1988*]. The content of phlogopite is widely variable, from a few percent to 40–80 %. The content of ilmenite ranges from a few percent to 15 %, rarely to 30–40 %. Mica and ilmenite contents sharply decrease in garnetized xenolithes, where these two minerals, as soon as olivine and pyroxenes are replaced by garnet. Euhedral, subhedral, sideronitic and porphyraceous textures in garnetless xenoliths are suggested the primary magmatic genesis of the rocks. In the series of Phl-Ilm hyperbasites, a special type of parageneses is represented by strongly deformed phlogopite-amphibole rocks with newly-formed chromite and relict resorbed ilmenite and clinopyroxene. The rocks of this series are also characterized by numerous autometasomatic and metasomatic reaction textures and wide ranges of modal mineral compositions: 0–80 % Grt, 1–40 % Ilm, 5–80 % Phl, 0–30 % Cpx, 10–70 % Opx, 0–40 % Ol, and 0.5–2.0 % Sulph. Amphibole occurs in garnetless parageneses and deformed phlogopite-amphibole rocks (with the newly formed chromite) in amounts of a few percent and up to 40–50 %, respectively.

The euhedral texture is essentially preserved in orthopyroxenites and partially websterites (Fig. 6, *A*). These rocks are composed of regular prismatic crystals of orthopyroxene which often have directive orientations. In olivine-containing xenoliths, large elongated crystals of olivine also formed partly idiomorphic crystals. Oval and round-shaped grains of olivine are often included into the grains of orthopyroxene less than into clinopyroxene without any traces of resorption (Fig. 6, *B*). The exsolution lamellae of clinopyroxene are commonly found in orthopyroxene from 10 to 15 % (Fig. 6, *B*). Besides, orthopyroxene contains numerous brownish micro-inclusions (5–20 μm) of ilmenite (≤1 %) which are regularly oriented and translucent (Fig. 6, *C*, *D*). Clinopyroxene- and ilmenite exsolution plates occupy central parts of orthopyroxene grains (almost ¾ of the area) and are absent in the marginal zones. The presence of the exsolution textures indicate an early high-temperature stage in the evolution of the rocks. Ilmenite and phlogopite form xenomorphic grains between earlier silicates without any evident reaction interrelations (Fig. 7, *A*, *B*) and belong to the late stage of magmatic crystallization. Inclusions of ilmenite in phlogopite occur as thin cleavage-oriented plates (≤1–5 μm) in the central parts of the grains or as oval-shaped blebs in the marginal parts (Fig. 7, *A*, *B*). Rare regular phlogopite flakes in orthopyroxene (Fig. 7, *C*, *D*) suggest that small amounts of mica were crystallized in some portions of the melt at the early magmatic stage.

In addition to evidence of typical magmatic genesis, phlogopite shows metasomatic relationships with primary silicates. In both the garnet-containing and garnetless parageneses, phlogopite forms 'windows' with abundant inclusions of small round-shaped grains of ilmenite and pyroxenes being relics of substitution (Fig. 8, *A*). Orthopyroxene crystals are grown through small irregular phlogopite flakes of the common optical orientation (Fig. 8, *B*, *C*). As shown in Fig. 9, *A*, *B*, orphopyroxene and clinopyroxene are intensively

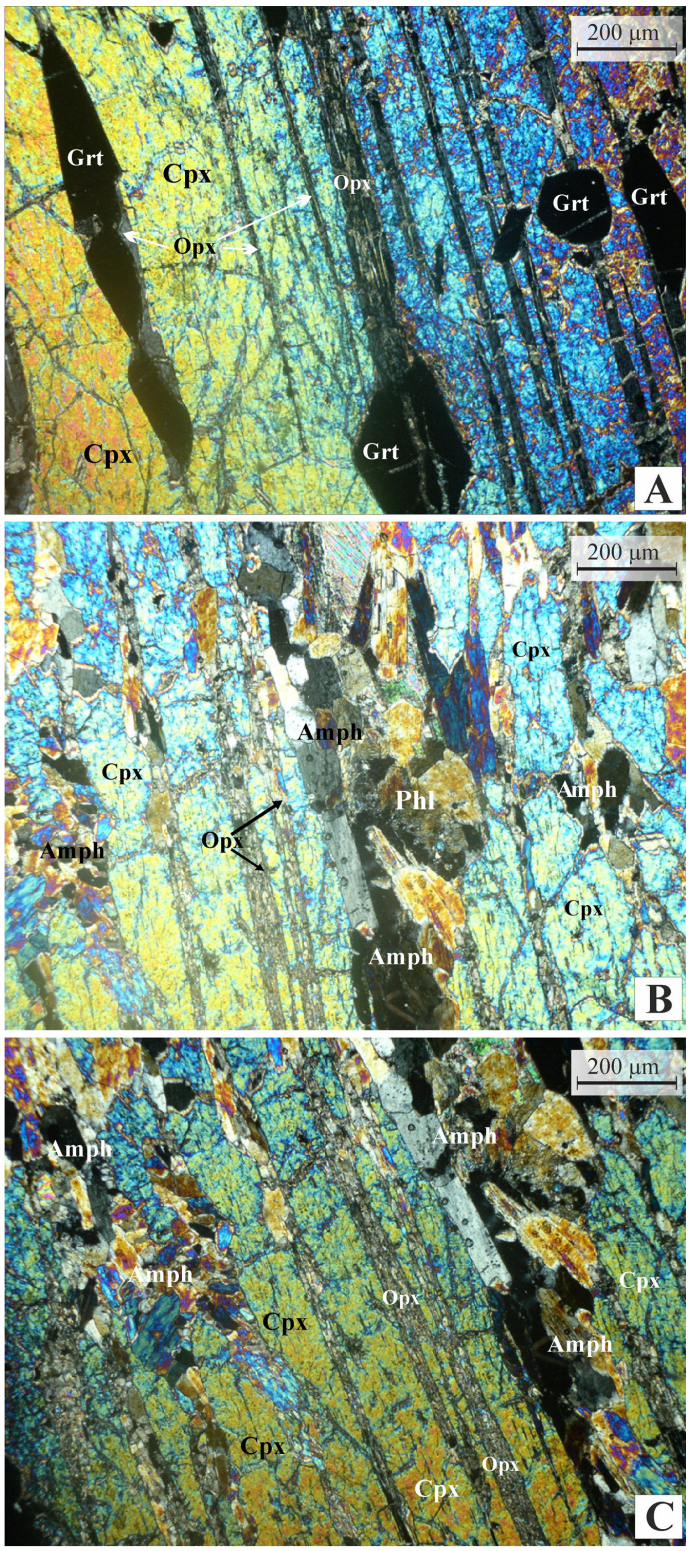


**Fig. 2.** The photomicrographs of thin section. Development of metasomatic Phl-Amph mineralization on orthopyroxene exsolution plates inside the clinopyroxene megacrystal in megacrystalline garnet websterite.

*A* – garnet and orphopyroxene exsolution plates inside the clinopyroxene megacrystal. Garnet is also developed in the form of isometric grains; *B, C* – fine-grained aggregate of Amph with rare plates of Phl, replacing mainly orphopyroxene exsolution plates. Images in crossed nicols.

**Рис. 2.** Развитие метасоматической Phl-Amph минерализации по пластинкам распада ортопироксена внутри мегакристалла клинопироксена в мегакристаллическом гранатовом вебстерите.

*A* – пластинки распада граната и ортопироксена в мегакристалле клинопироксена, гранат развит также в виде изометричных зерен; *B, C* – мелкозернистый агрегат Amph с редкими пластинками Phl, развивающийся преимущественно по пластинкам распада ортопироксена. Фото шл. в × николях.

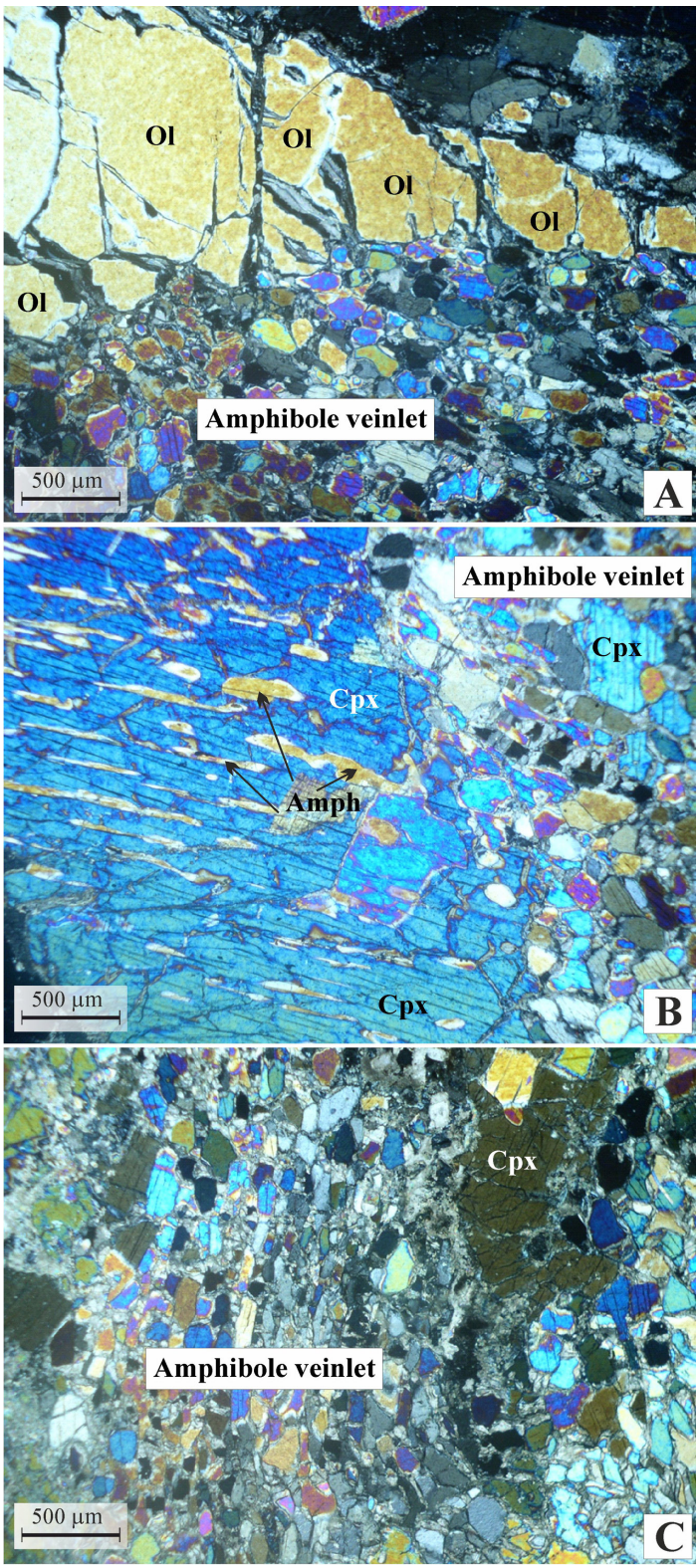


**Fig. 3.** The photomicrographs of thin section. Amphibole veinlets with rare phlogopite plates in Grt olivine websterite (sample 74-817).

*A* – resorption of the olivine grain at the contact with the amphibole veinlet; *B* – oriented elongated crystals of amphibole developing in the clinopyroxene grain from the boundary of the amphibole veinlet; *C* – relics of the clinopyroxene grain in selvage of the amphibole veinlet. Images in crossed nicols.

**Рис. 3.** Амфиболовые прожилки с редкими пластинками флогопита в Grt оливиновом вебстерите (обр. 74-817).

*A* – резорбция зерна оливина на контакте с амфиболовым прожилком; *B* – ориентированные удлиненные кристаллы амфибола, развивающиеся в зерне клинопироксена от границы амфиболового прожилка; *C* – реликты зерен клинопироксена в зольбандах амфиболового прожилка. Фото шл. в × николях.

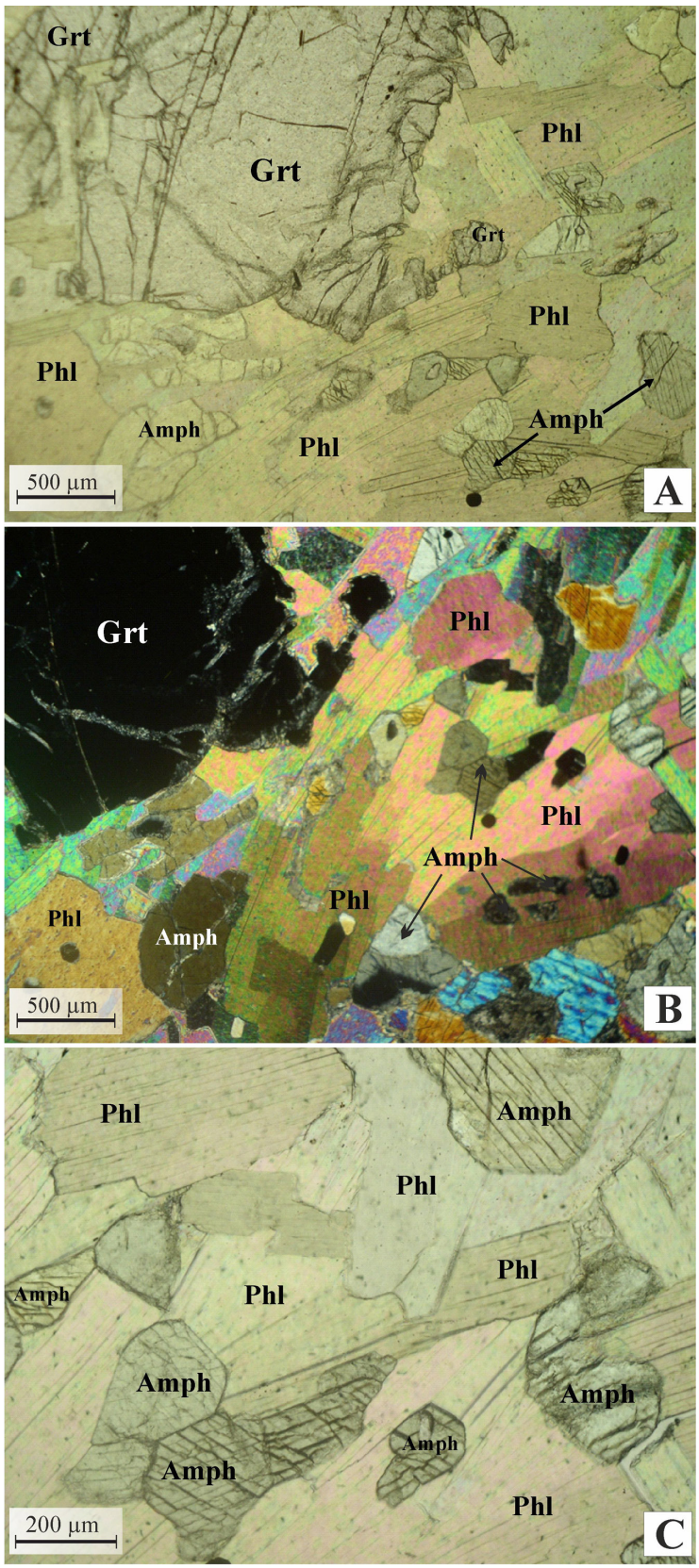


**Fig. 4.** *A, B* – the photomicrographs of thin section. Resorption of the garnet grain by phlogopite at the boundary with the phlogopite-amphibole veinlet; *C* – the area of the phlogopite-amphibole veinlet with dominating phlogopite.

Cross-sections of regular amphibole crystals are visible. Sample 74-817. Images: *A, C* – without an analyzer; *B* – in crossed nicols.

**Рис. 4.** *A, B* – резорбция зерна граната флогопитом на границе с флогопит-амфиболовым прожилком; *C* – участок флогопит-амфиболового прожилка с преобладанием флогопита.

Видны сечения правильных кристаллов амфибола. Обр. 74-817. Фото шл.: *A, C* – без анализатора; *B* – в × николях.

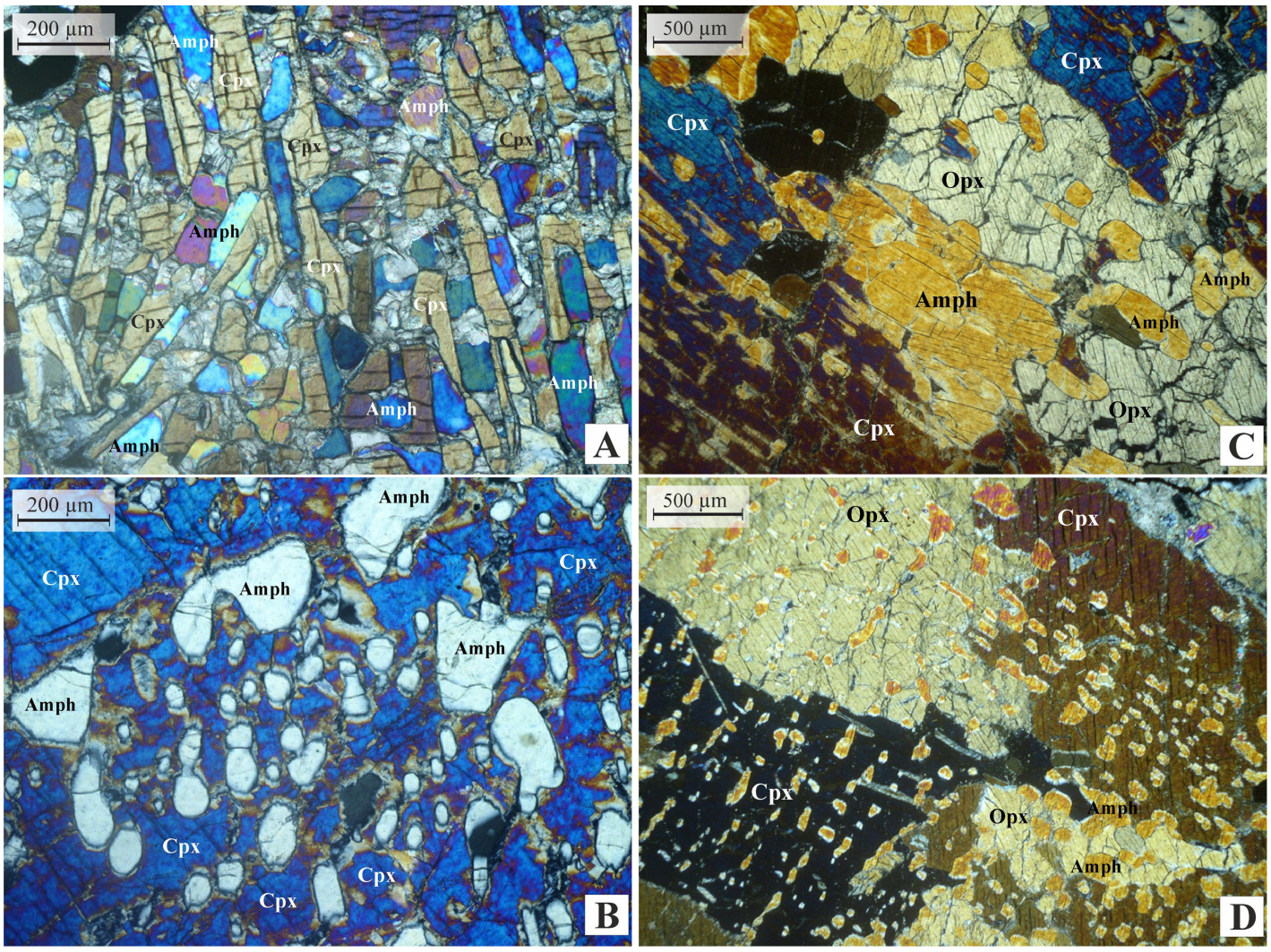


**Fig. 5.** The photomicrographs of thin section. The abundant development of metasomatic amphibole in clinopyroxene grains.

*A* – small elongated crystals of amphibole in the clinopyroxene grain (Cpx – cross-section with transversal cleavage and yellow interference colour); *B* – drop-like grains of amphibole (white interference colour) which have single crystallographic orientation in the clinopyroxene grain (blue interference colour). *C* – elongated crystals of amphibole with similar spatial and crystallographic orientation in different grains of clinopyroxene. *D* – small grains of amphibole crossing different grains of clinopyroxene in two mutually perpendicular directions. Sample 74-817. Images in crossed nicols.

**Рис. 5.** Массовое развитие метасоматического амфибола в зернах клинопироксена.

*A* – мелкие удлиненные кристаллы амфибола в зерне клинопироксена (Cpx – разрез с пересекающейся спайностью и с желтой интерференционной окраской); *B* – каплевидные зерна амфибола (белая интерференционная окраска), имеющие единую оптическую ориентировку в зерне клинопироксена – синяя интерференционная окраска; *C* – удлиненные кристаллы амфибола с одинаковой пространственной и оптической ориентировкой в разных зернах клинопироксена. *D* – мелкие зерна амфибола, пересекающие разные зерна клинопироксена по двум взаимно перпендикулярным направлениям. Обр. 74-817. Фото шл. в × николях.

replaced by phlogopite, and clinopyroxene is reactionnary developing at the earlier grain of orphopyroxene. In many cases, reaction phlogopite develops in the form of palmate porphyroblasts with inclusion of pyroxene and olivine relics (Fig. 9, *C*, *D*). Small zonal plates occuring in fractures of the rocks in the paragenesis with carbonate belong to the later stage and are associated with the influence of the kimberlitic melt on the xenolith (Fig. 10, *A*, *B*).

The most complex relationships are revealed between phlogopite and garnet. The development of garnet at the subsolidus stage is evidenced by the fact that garnet inventively replaced minerals of the primary paragenesis, including phlogopite. In some xenoliths, garnet is dominant, and its content may exceed 80 %. Garnet grains are filled by relics of substituted minerals of the earlier paragenesis, such as Ol, Opx, Cpx, Ilm and Phl (Fig. 11, *A*, *B*), and have a typical sieve-like

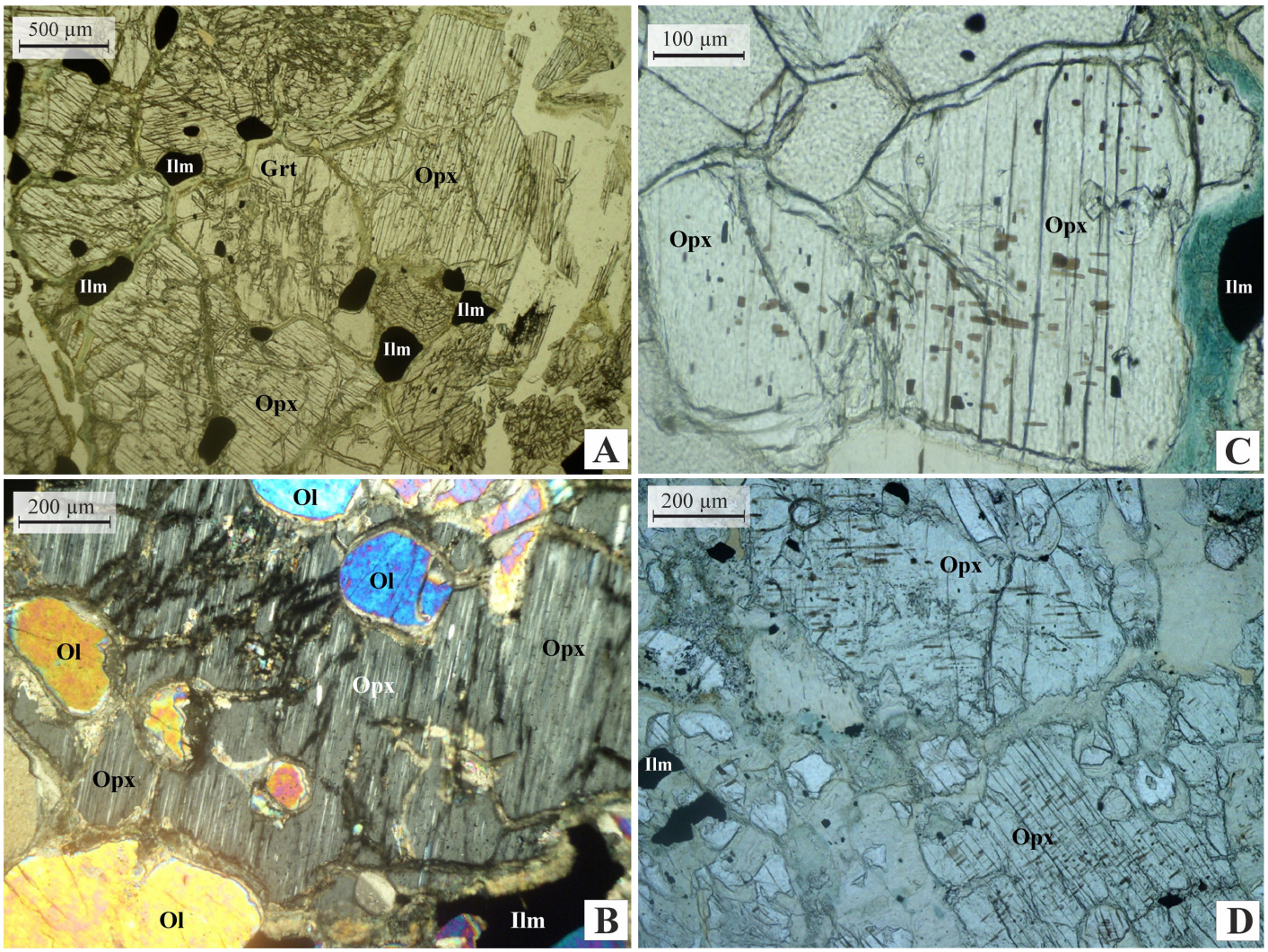


**Fig. 6.** The photomicrographs of thin section. Relationships between minerals in Phl-Ilm hyperbasites.

*A* – euhedral texture formed by prismatic crystals of orthopyroxene which are separated by irregular-shaped oval grains of ilmenite; *B* – roundish olivine inclusions in the orthopyroxene grain (homoaxial pseudomorphs). Clinopyroxene exsolution textures are visible in orthopyroxene (parallel light-coloured strips); *C, D* – submicroscopic structures of ilmenite exsolution textures in orthopyroxene. Images: *A, C, D* – without an analyzer; *B* – in crossed nicols.

**Рис. 6.** Взаимоотношения минералов в Phl-Ilm гипербазитах.

*A* – панидиоморфнозернистая структура, образованная призматическими кристаллами ортопироксена, между которыми расположены неправильные овальные зерна ильменита; *B* – округлые включения оливина в зерне ортопироксена (гомоосевые псевдоморфозы). В ортопироксене видны структуры распада клинопироксена (параллельные светлые полоски); *C, D* – субмикроскопические структуры распада ильменита в ортопироксене. Фото шл.: *A, C, D* – без анализатора; *B* – в × николях.

fabric in the crossed nicols (Fig. 11, *B*). In the rocks, garnet forms gatherings of round-shaped grains with partial faceting, which are mainly associated with clusters of phlogopite grains. Phlogopite relics are contained in the garnet grains as irregular-shaped or ribbon-shaped inclusions connected with the phlogopite rim at the margins of the garnet grains (Fig. 12, *A*, *B*). Figure 13 shows the replacement of the orphopyroxene grain by the phlogopite plate; the orphopyroxene grain is surrounded by garnet that is reactionary replacing orphopyroxene. Amounts of ilmenite and phlogopite are significantly decreased in the garnetization areas, to suggest the preferred development of garnet on these minerals. Numerous small-sized roundish and semi-faceted hexagonal crystals of pyroxenes, ilmenite and rare phlogopite (Fig. 14, *A*, *B*, *C*) fill the central parts of garnet grains, while the rim of the grains remains free of inclusions. Relict grains of clinopyroxene and orthopyroxene in garnet are often characterized by single extinction to evidence their primary belonging to the same grain. The pseudo-hexagonal faceting of the inclusions is due to the effect of garnet

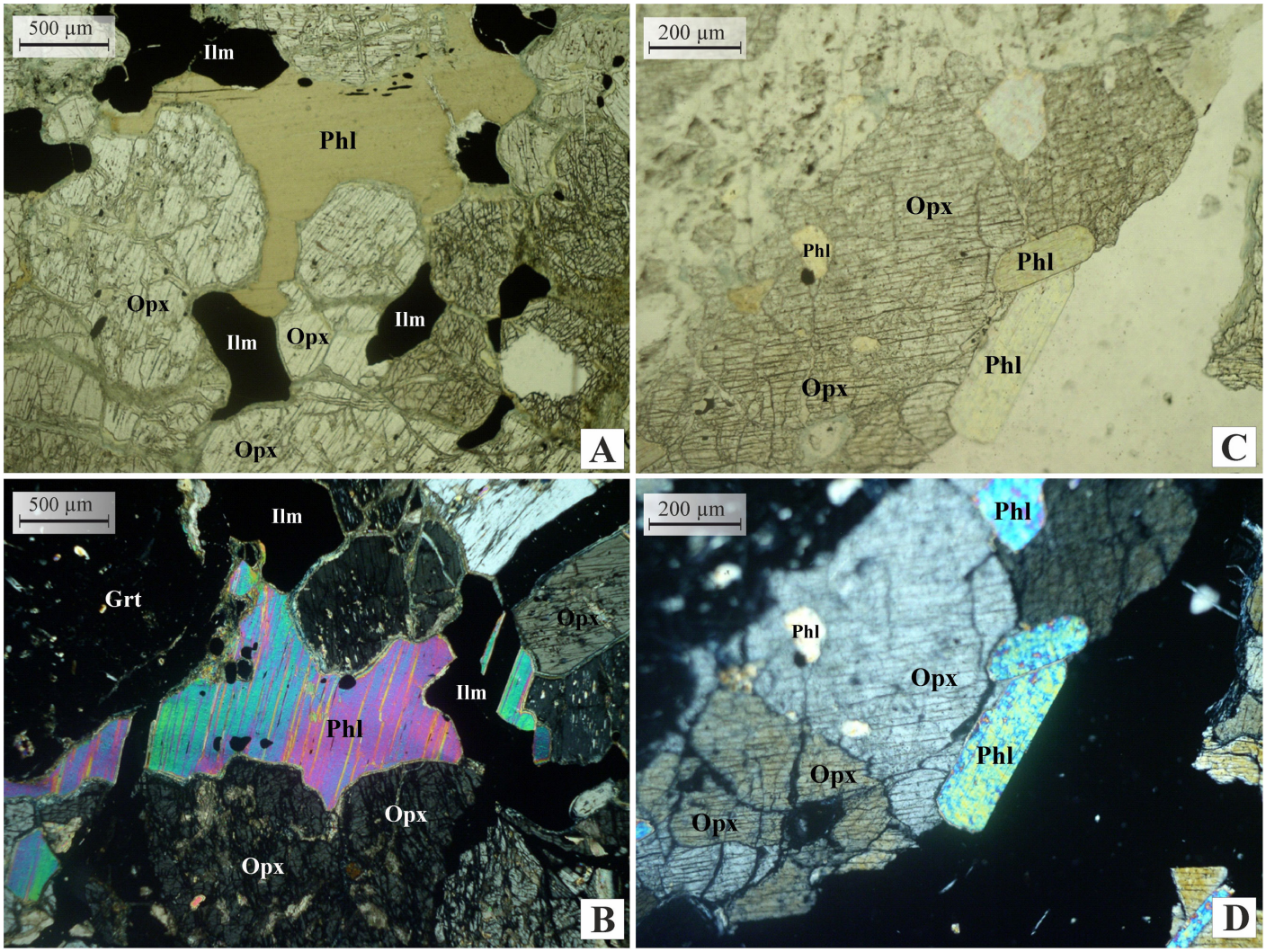


**Fig. 7.** The photomicrographs of thin section. Relationships between minerals in Phl-Ilm hyperbasites.

*A, B* – irregular palmate plates of phlogopite and smaller irregular grains of ilmenite between grains of idiomorphic orthopyroxene. Thin (≤5 μm) elongated ilmenite lamellae are present in the phlogopite plates. Larger oval ilmenite grains are associated with margins of the plates; *C, D* – small regular Phl platelets in the orthopyroxene grain. Images: *A, C* – without analyzer; *B, D* – in crossed nicols.

**Рис. 7.** Взаимоотношения минералов в Phl-Ilm гипербазитах.

*A, B* – неправильные лапчатые пластинки флогопита и более мелкие неправильные зерна ильменита между зернами идиоморфного ортопироксена. В пластинках флогопита отмечаются тонкие (≤5 мкм) длинные пластинки ильменита. К краям пластинок приурочены более крупные овальные зерна ильменита; *C, D* – правильные мелкие пластинки Phl в зерне Opx. Фото шл.: *A, C* – без анализатора; *B, D* – в × николях.

crystallographic structure.

It should be noted also that evidences of the development of phogopite on garnet are revealed in the garnetized rocks. The boundary between large irregular mica plates and garnet grains has often resorption character (Fig. 15, *A*, *B*). The two minerals often form mutual gulf-shaped boundaries. Roundish inclusions of ilmenite and silicates are visible in garnet. In the centre of the mica flakes there are thin ilmenite platelets, in the margins the ilmenite form roundish inclusions (Fig. 15, *B*). Resorbed garnet relics, that may have been separated from a larger grain, occur in phlogopite (Fig. 16, *A*, *B*). Inclusions of garnet grains in the phlogopite plate (Fig. 16, *C*, *D*) can also be explained by replacing of garnet by phlogopite, though such a conclusion is ambiguous. As evidenced by the above-described observations, relationships between phlogopitization and garnetization are complicated. Obviously, both processes took place at the late stage of rock crystallization and, most probably, at the subsolidus stage when the major part of the minerals was crystallized. The leading role of temperature drop in the development of phlogopite and garnet is suggested by relatively weak signs of deformation, such as insignificantly bending of

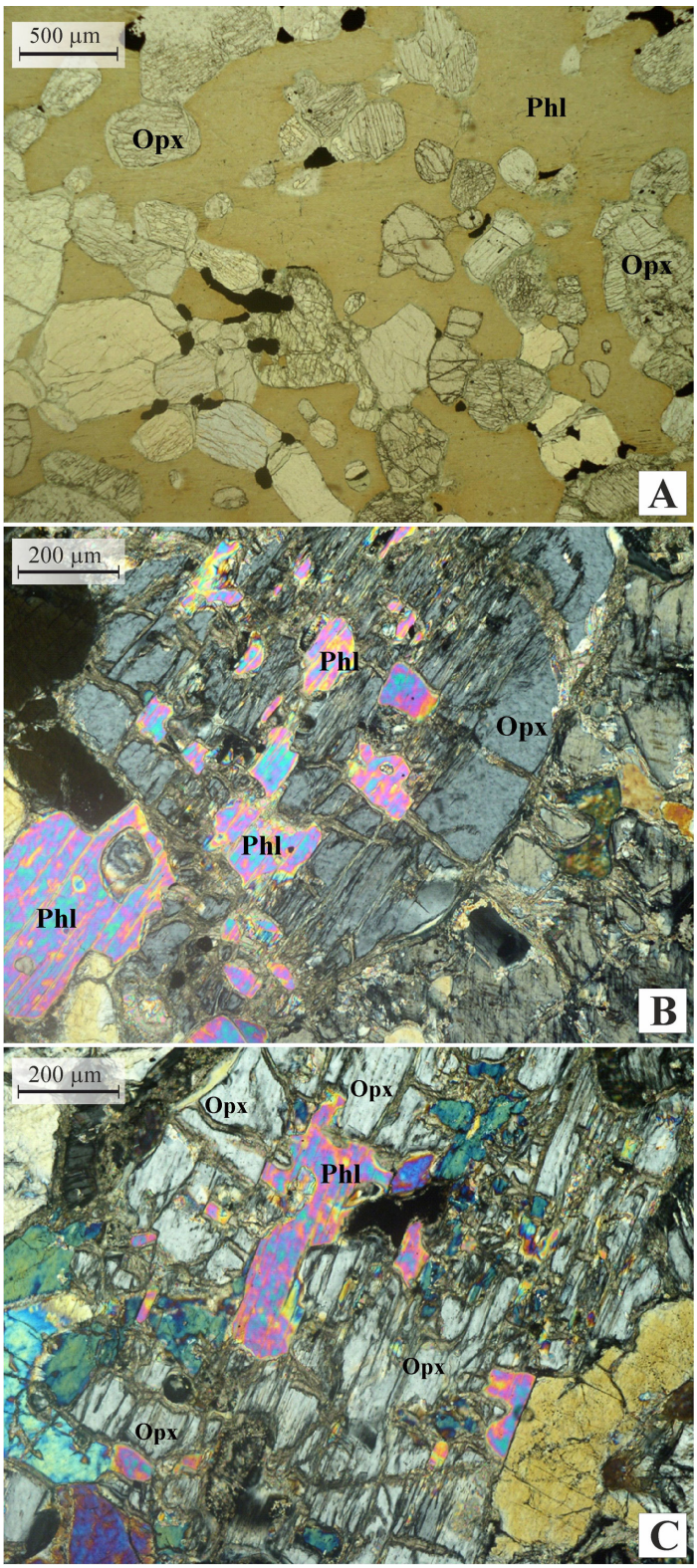


**Fig. 8.** The photomicrographs of thin section. The character of the metasomatic phlogopite development.

*A* – metasomatic phlogopite forms 'windows' in the rocks. The large mica plate contains abundant relics of olivine and pyroxenes and resorbed grains of ilmenite (black); *B, C* – intensive phlogopitization of orthopyroxene grains: phlogopite develops in the form of irregular plates with the single crystallographic orientation. Images: *A* – without an analyzer; *B, C* – in crossed nicols.

**Рис. 8.** Характер развития метасоматического флогопита.

*A* – заполнение метасоматическим флогопитом участков, своеобразных «окон» в породе. Крупная пластинка слюды содержит обильные реликты оливина, пироксенов и резорбированных зерен ильменита (черное); *B, C* – интенсивная флогопитизация зерен ортопироксена: флогопит развивается в виде неправильных пластинок с единой оптической ориентировкой. Фото шл.: *A* – без анализатора; *B, C* – в × николях.

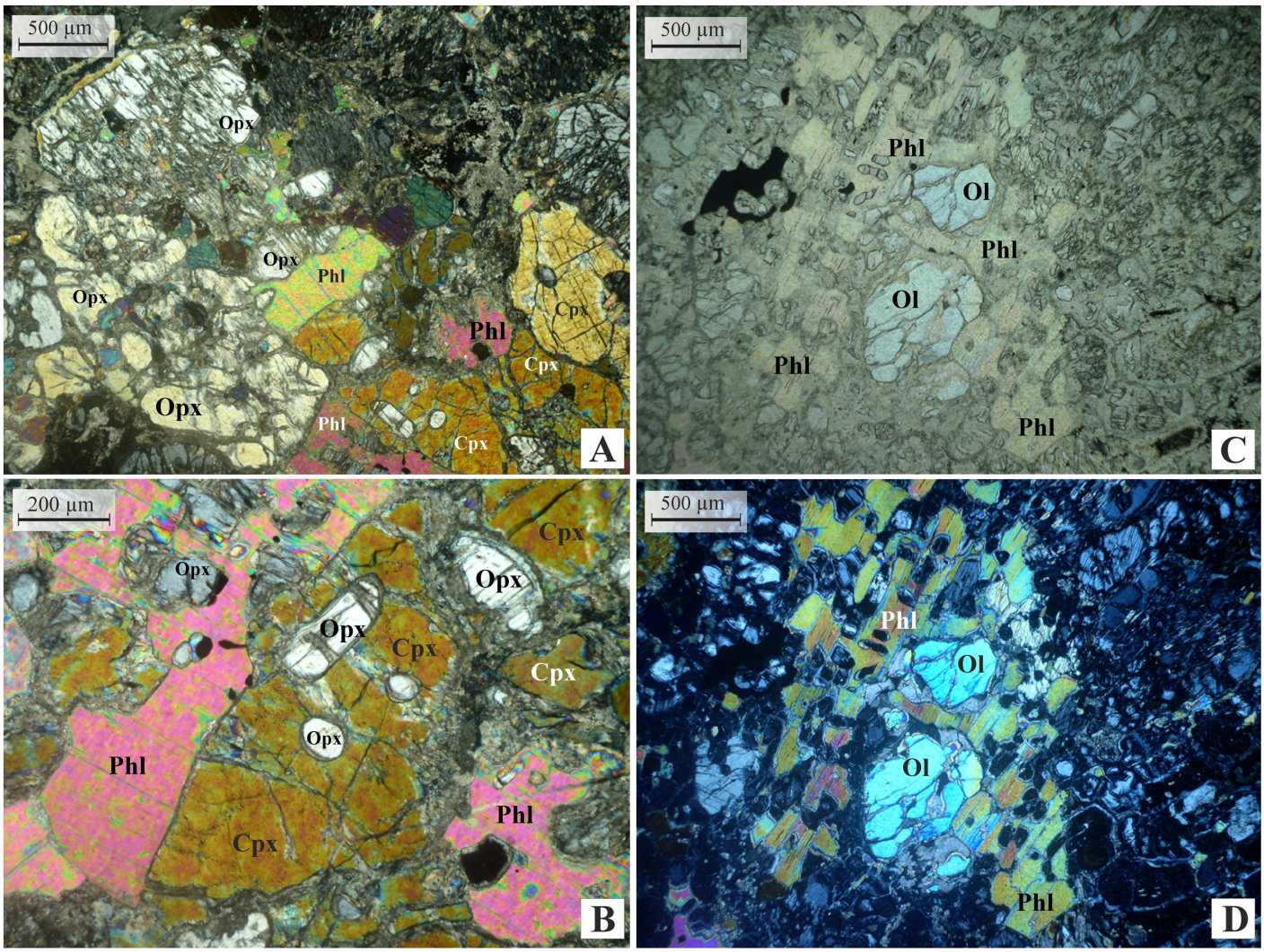


**Fig. 9.** The photomicrographs of thin section. Reaction development of phlogopite on primary minerals.

*A, B* – the irregular plate of phlogopite, corroding the grains of orthopyroxene and clinopyroxene; *B* – clinopyroxene develops on orthopyroxene and is replaced by Phl; *C, D* – unregular porphyroblastic plate of phlogopite contains relics of replaced grains of orthopyroxene and olivine. Images: *A, B, D* – in crossed nicols; *C* – without an analyzer.

**Рис. 9.** Реакционное развитие флогопита по первичным минералам.

*A, B* – неправильная пластинка флогопита, разъедающая зерна ортопироксена и клинопироксена; *B* – клинопироксен, развивающийся по ортопироксену и замещающийся Phl. В зерне Cpx и в пластинке Phl сохранились одинаково гаснущие реликты зерен Opx; *C, D* – неправильная порфиробластическая пластинка флогопита, содержащая реликты замещенных зерен ортопироксена и оливина, два разобщенных реликта которого имеют одинаковую оптическую ориентировку. Фото шл.: *A, B, D* – в × николях; *C* – без анализатора.

phlogopite plates and slightly undulate extinction of olivine. Phlogopite seems to be formed in the latest magmatic stage from rich in potassium and volatiles residual melts, and later from fluids during autometasomatism. Relationships between garnet and phlogopite are complicated as phlogopitization and garnetization developed almost simultaneously with some advance occurrences of one process in local areas. Residual melt-fluids rich in potassium and volatile components are evidenced by the Phl-Ilm garnetless parageneses with high contents of phlogopite and ilmenite (30–80 % and 15–40 %, respectively). Phlogopite occurs in large porphyraceous plates and fine platelets of the second generation in the fine-grained matrix (Fig. 17, 18). Sometimes ilmenite grains have ideal facets and belong to the matrix paragenesis (Fig. 18, *A*). The specific features of porphyraceous phlogopite I are ilmenite thin regularly-oriented lamellae in the centre and larger roundish ilmenite grains in the marginal zones (Fig. 19, *A*, *B*). The outside rims of phlogopite I and the platelets in the matrix are more intensely brown-coloured (Fig. 20, *A*–*E*). In rare cases, garnet occurs in the

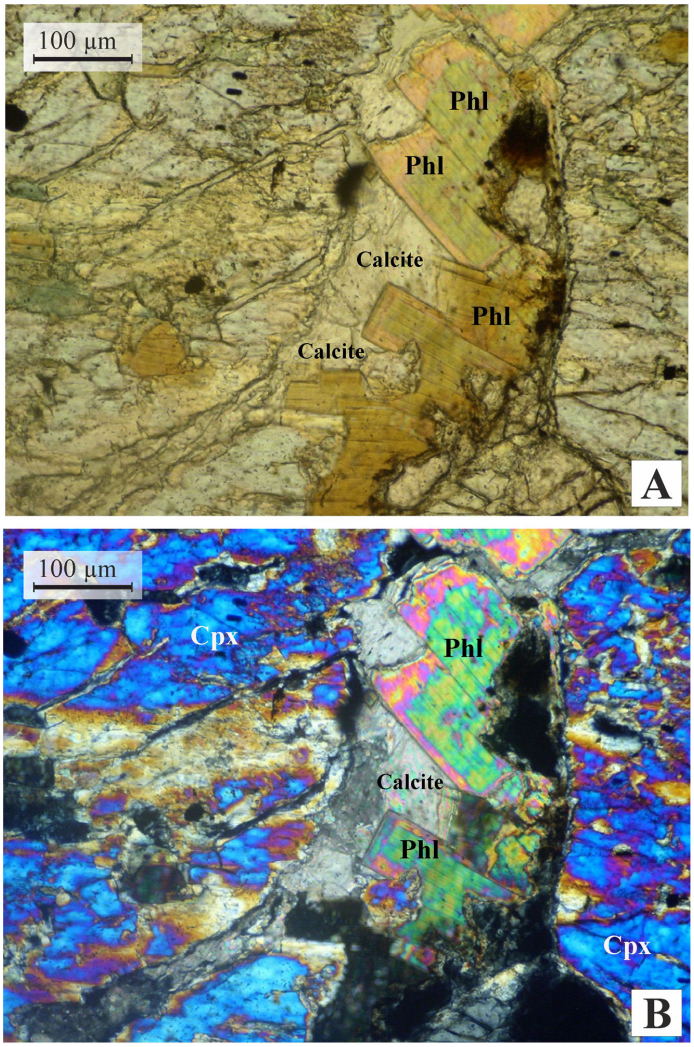


**Fig. 10.** The photomicrographs of thin section. Late paragenesis of phlogopite with carbonate, which develops along the fractures in the rock.

Regular phlogopite platelets grow on the fracture wall. Phlogopite is almost colourless in narrow rims of the plates. Images: *A* – without an analyzer; *B* – in crossed nicols.

**Рис. 10.** Поздний парагенезис флогопита с карбонатом, развивающийся по трещинкам в породе.

Правильные пластинки флогопита нарастают на стенку трещинки. В узких краях пластинок флогопит почти бесцветен. Фото шл.: *A* – без анализатора; *B* – в × николях.

form of accessory strongly resorbed grains. The garnet grain is filled in with abundant inclusions of roundish ilmenite grains that are relics of substitution (Fig. 20). The garnet grain seem to be trapped by the melts from the earlier crystallized intrusive phase. The sieve-like structure of the garnet grains with abundant pseudohexagonal and isometric relics of pyroxenes, ilmenite and, in some cases, phlogopite suggests that garnet developed mainly in the solid rock after crystallization of all the magmatic minerals. Quite possibly, a part of garnets might have formed at the late stages of crystallization of the melt portions located in the zone of garnet facies. This can be suggested from rare xenoliths of

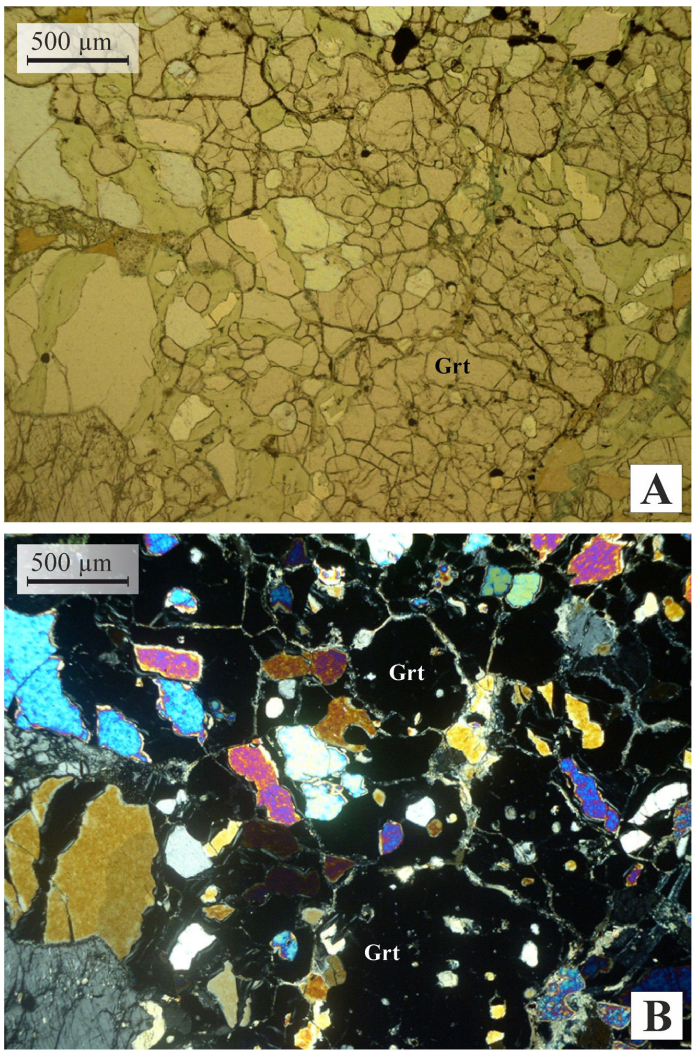


**Fig. 11.** The photomicrographs of thin section. The abundant development of garnet in the xenolith of the Phl-Ilm garnetized lherzolite.

Numerous relics of minerals of the early paragenesis, such as olivine, pyroxenes, ilmenite and phlogopite, are present inside the garnet grains. Images: *A* – without analyzer; *B* – in crossed nicols. The separate grains of garnet (black) with thin light-coloured margins are visible. Irregular silicates relics are coloured in different interference colours and included in garnet or located at the boundaries of the garnet grains.

**Рис. 11.** Массовое развитие граната в ксенолите Phl-Ilm гранатизированного лерцолита.

Внутри зерен граната сохранились многочисленные реликты минералов раннего парагенезиса – оливина, пироксенов, ильменита и флогопита. Фото шл.: *A* – без анализатора; *B* – в × николях. Видны отдельные зерна граната (черное), окаймленные тонкими светлыми каймами. Неправильные реликты силикатов окрашены в разные интерференционные цвета и включены в гранат или расположены на границах его зерен.

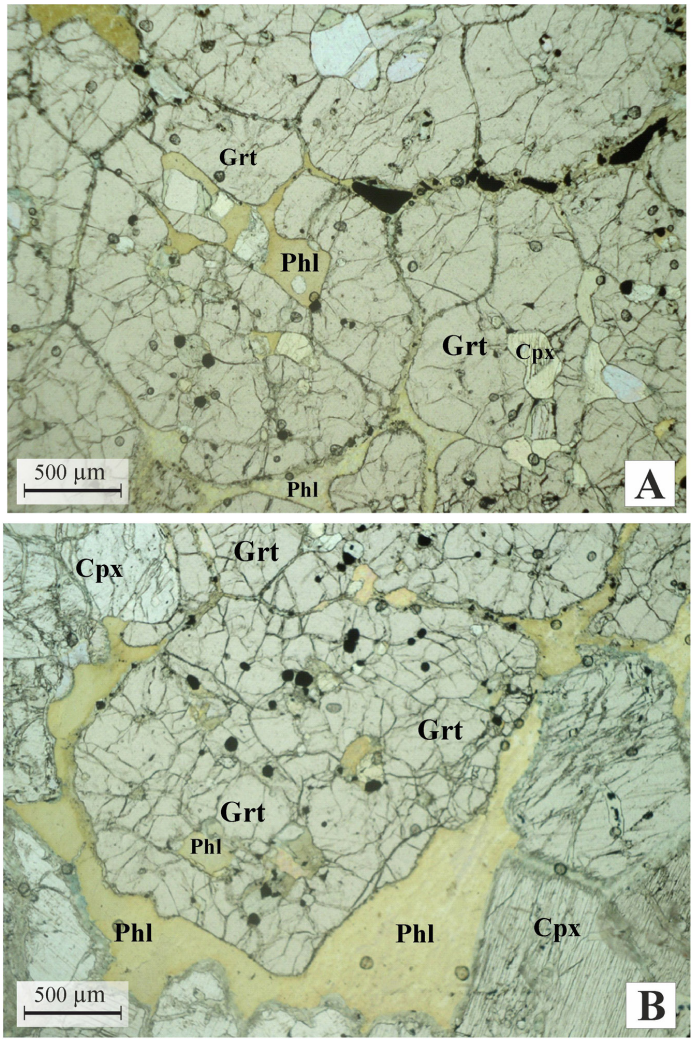


**Fig. 12.** The photomicrographs of thin section. Polycrystalline aggregate composed of garnet regular grains in the Phl-Ilm garnetized lherzolite (*A, B*).

Garnet mainly developed on phlogopite which ribbon-shaped relics are connected with the external rim. Phlogopite in garnet and the rim have single crystallographic orientations. Besides phlogopite, roundish relics of ilmenite (black) and silicates are visible in the garnet grains. Image (*A*) shows larger elongated ilmenite grains which were 'forced out' to the margins of the garnet grains. Images without an analyzer.

**Рис. 12.** Поликристаллический агрегат из правильных зерен граната в Phl-Ilm гранатизированном лерцолите (*A, B*).

Гранат развит преимущественно по флогопиту, от которого остались лентовидные реликты, соединяющиеся с внешней каймой. Флогопит в гранате и кайма имеют одинаковую оптическую ориентировку и до гранатизации составляли единое зерно. Кроме флогопита в зернах граната видны округлые реликты ильменита (черное) и силикатов. На (*A*) видны более крупные удлиненные зерна ильменита, «вытесненные» на края зерен граната. Фото шл. без анализатора.

orthopyroxenites with very insignificant quantities of phlogopite, wherein garnet forms small regular-shaped grains between the grains of orthopyroxene and does not contain any substitution relics of other minerals.

The deformed phlogopite-amphibole rocks contain regular-shaped microcrystals (5–50 µm) of titanian chromite and resorbed relict grains of ilmenite (3–7 %) and clinopyroxene (≤5 %) (Fig. 21, *A*, *B*). Particular texture features evidence that the rocks were formed under conditions of strong deformation. Elongated prismatic amphibole crystals form narrow rosettes intergrown with strongly deformed irregular-shaped plates of phlogopite (Fig. 22, *A–E*). The amphibole crystals are often bended. Inside the phlogopite grains, they look like torn-off relics. Cross-sections of phlogopite resemble a torchs or a quadrangular stars with sharp torn-off edges (Fig. 22, *C*, *D*; Fig. 23, *A*). The phlogopite plates are strongly deformed and dissected into blocks of various orientations that are healed by a fine-grained aggregate of more intensively coloured mica (Fig. 23, *A–D*). The ilmenite inclusions are lacking in the phlogopite. In the rocks, ilmenite occurs as elongated irregular-shaped grains with serrated edges indicating its dissolution (Fig. 21, *A*, *B*). Aggregates of prismatic amphibole are associated with micrograins of titanian chromite. Specific textures and mineral compositions of the deformed phlogopite-amphibole rocks suggest

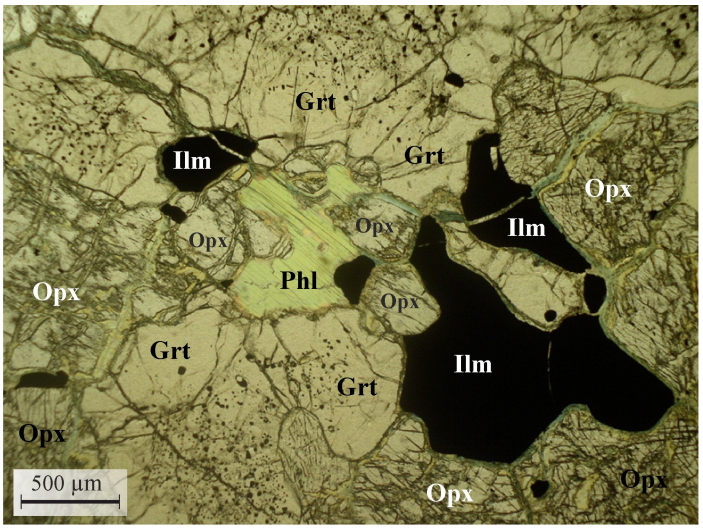


**Fig. 13.** The photomicrographs of thin section. The irregular Phl plate developing on the Opx grain that is surrounded by growing garnet grain.

Central parts of the Grt grain contain relics of ilmenite (black points). At the right of the image, a gulf-like extension of the garnet cuts the large grain of ilmenite. Image without an analyzer.

**Рис. 13.** Неправильная пластинка Phl, развивающаяся по зерну Opx, окруженному зернами разрастающегося граната.

Центральные части зерен Grt испещрены черными точками (реликты Ilm). В правой части фото видно, как заливообразное продолжение зерна граната расчленяет крупное зерно ильменита. Фото шл. без анализатора.

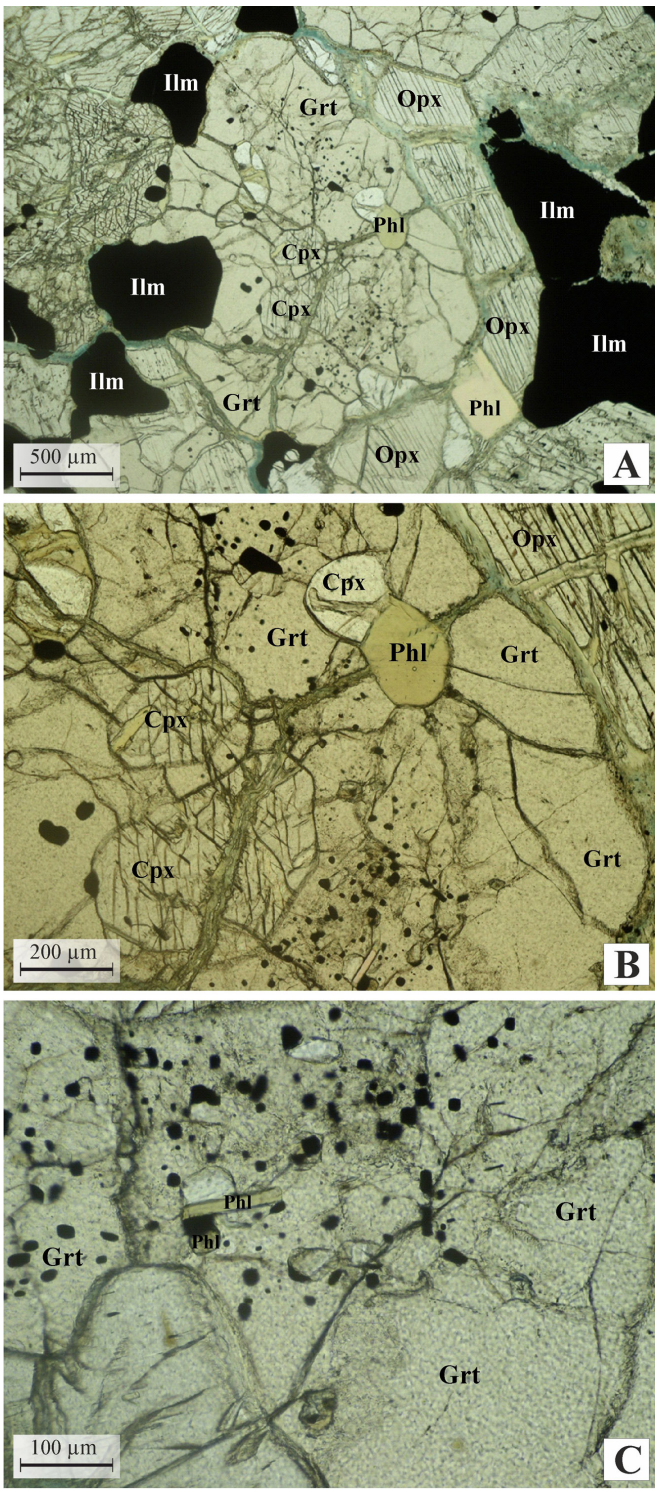


**Fig. 14.** The photomicrographs of thin section. The garnet porphyroblast has regular crystallographic facets and develops on the orthopyroxene grain in the Phl-Ilm garnetized websterite.

*A, B* – inside garnet, visible are numerous semi-faceted pyroxene grains, small roundish grains of ilmenite and a hexagonal platelets of phlogopite. In external zone of the garnet porphyroblast, inclusions of relics of other minerals are lacking. In the rock large grains of ilmenite are irregularly shaped. *B* – small regular platelets of phlogopite in the garnet porphyroblast. Images (*B*) and (*C*) show zoomed-up areas given in image (*A*). Images without an analyzer.

**Рис. 14.** Порфиробласт граната, имеющий правильную кристаллографическую огранку и развивающийся по зерну ортопироксена в Phl-Ilm гранатизированном вебстерите.

*A, B* – внутри граната видны многочисленные полуограненные зерна пироксенов, округлые мелкие зерна ильменита и гексагональная пластинка флогопита. Во внешней зоне порфиробласта граната включения реликтов других минералов отсутствуют. Крупные зерна ильменита в породе имеют обычно неправильную форму и размеры. *C* – мелкие правильные пластинки флогопита в порфиробласте граната. *B* и *C* – увеличенные участки (*A*). Фото шл. без анализатора.

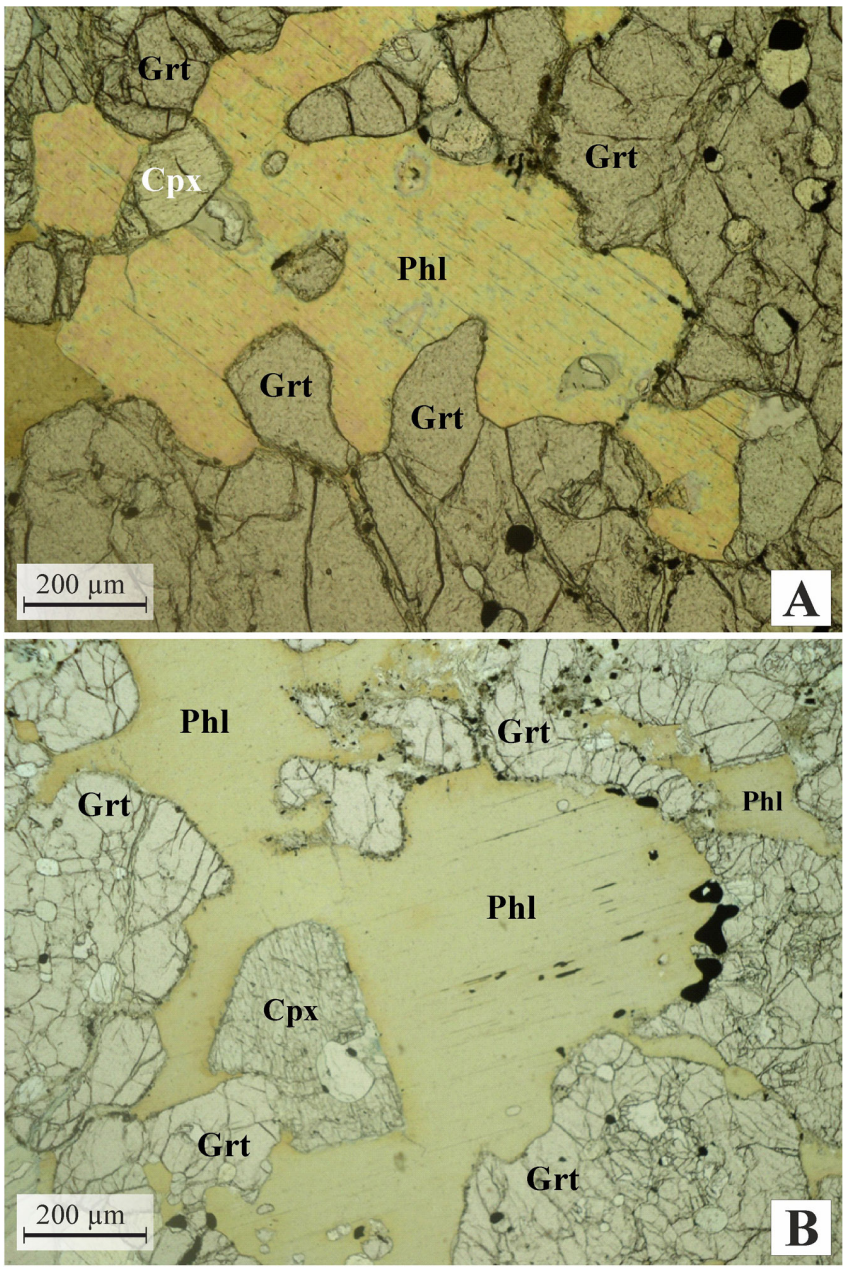


**Fig. 15.** The photomicrographs of thin section. Reaction boundaries between garnet and phlogopite in the Phl-Ilm garnetized lherzolite.

Grains of both minerals are irregularly shaped and have gulf-like mutual boundaries. Relics of ilmenite and silicates are visible in garnet in images (*A*) and (*B*). In central parts of the phlogopite plate, long thin ilmenite lamellae are oriented along cleavage; at the boundary of the plate, they change to larger oval grains (*B*). Images without an analyzer.

**Рис. 15.** Реакционные границы между гранатом и пластинками флогопита в Phl-Ilm гранатизированном лерцолите.

Формы зерен того и другого минерала неправильные, с заливообразными взаимными вхождениями. В гранате видны округлые реликты ильменита и силикатов (*A, B*). В центральных частях пластинок флогопита по спайности ориентированы тонкие длинные пластинки ильменита, которые сменяются на границе зерна более крупными овальными зернами (*B*). Фото шл. без анализатора.

their formation under conditions of intensive stress, possibly, in the root parts of deep faults.

The described petrographic features of the ilmenite-phlogopite parageneses in the deep-seated xenoliths from the kimberlites of the Kuoika field are the basis for the following conclusions:

1. The xenoliths of the Phl- Ilm hyperbasites are pieces of the complex mantle magmatic complex characterised by ubiquitous subsolidus metasomatic processes. The primary magmatic origin of the series is

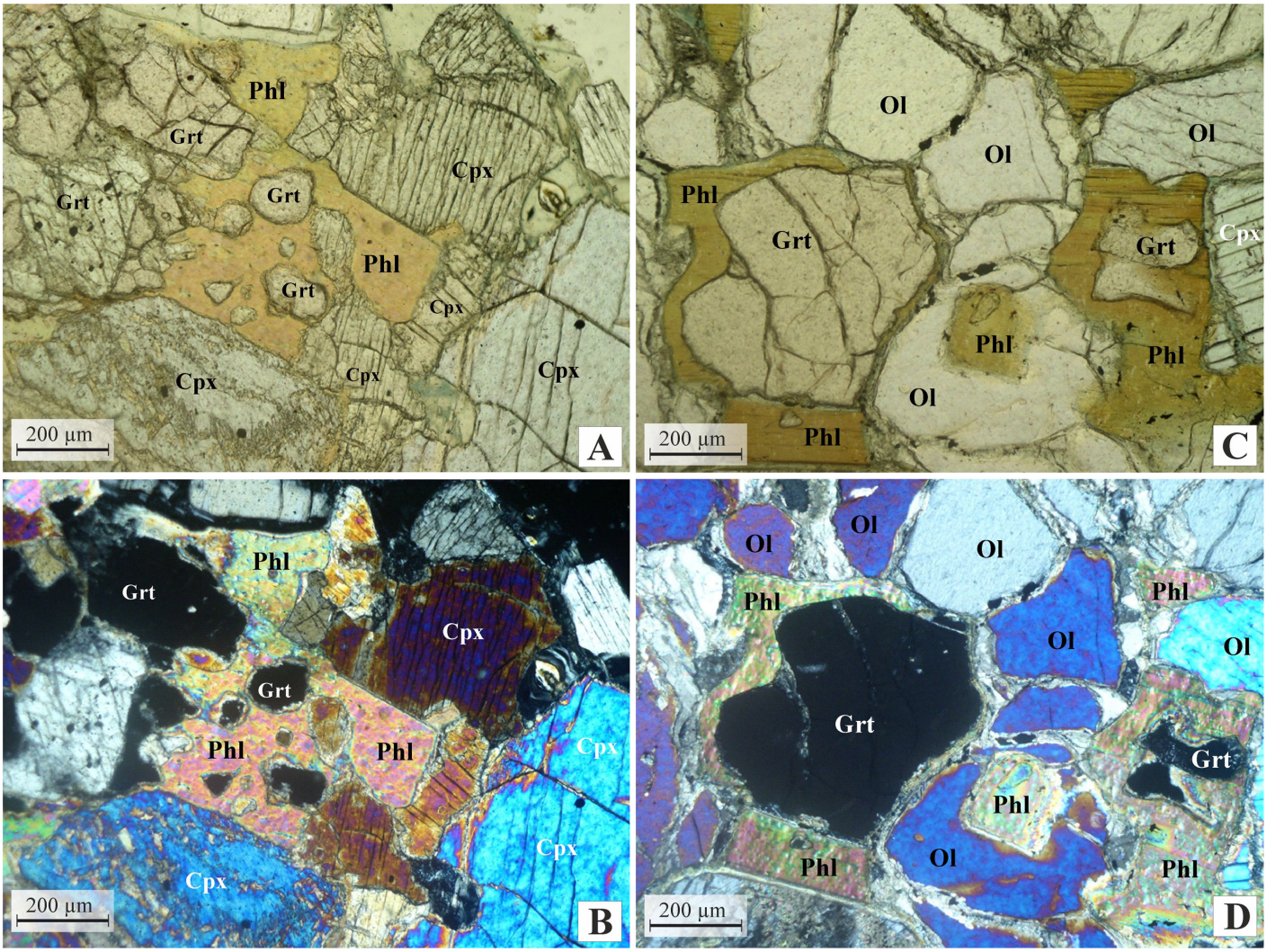


**Fig. 16.** The photomicrographs of thin section. Reaction relationships between garnet and phlogopite in the Phl-Ilm garnetized clinopyroxenite.

Images (*A*) and (*B*) show that the resorbed part of the clinopyroxene crystal and small grains of garnet (possibly, separated from a larger grain) are present in the phlogopite plate. Boundaries between mica and clinopyroxene and garnet have reaction character. Images (*C*) and (*D*) show isometric grains of garnet in phlogopite plate. In this case, it is impossible to unambiguously determine either phlogopite developed later than garnet or vice versa. Images: *A, C* – without an analyzer; *B, D* – in crossed nicols.

**Рис. 16.** Реакционные взаимоотношения между гранатом и флогопитом в Phl-Ilm гранатизированном клинопироксените.

(*A, B*) в пластинке флогопита находятся резорбированная часть кристалла клинопироксена и мелкие зерна граната, возможно, отделенные от более крупного зерна. Границы слюды с клинопироксеном и гранатом имеют реакционный характер. (*C, D*) изометричные зерна граната в пластинках флогопита. Разобщенные пластинки флогопита принадлежат единому зерну, о чем свидетельствует их одинаковое погасание. В данном случае нельзя однозначно судить о более позднем развитии флогопита по отношению к гранату или наоборот. Фото шл.: *A, C* – без анализатора; *B, D* – в × николях.

confirmed by the magmatic sequence of crystallization of the minerals (olivine – orthopyroxene – clinopyroxene with late phlogopite and ilmenite) and the presence of typical magmatic (euhedral, subhedral, sideronitic and porphyraceous) structures.

2. The intensive substitution of the minerals by phlogopite took place, most probably, at the subsolidus stage during the process of autometasomatism when the early intrusive phases were affected by late melts rich in potassium and volatiles. The complex morphological relationships between phlogopite and garnet developing at the given stage suggest their simultaneous occurrence with the advance development of either phlogopitization or garnetization in the local areas of the rocks.

3. The next evolution stage of the Phl-Ilm series

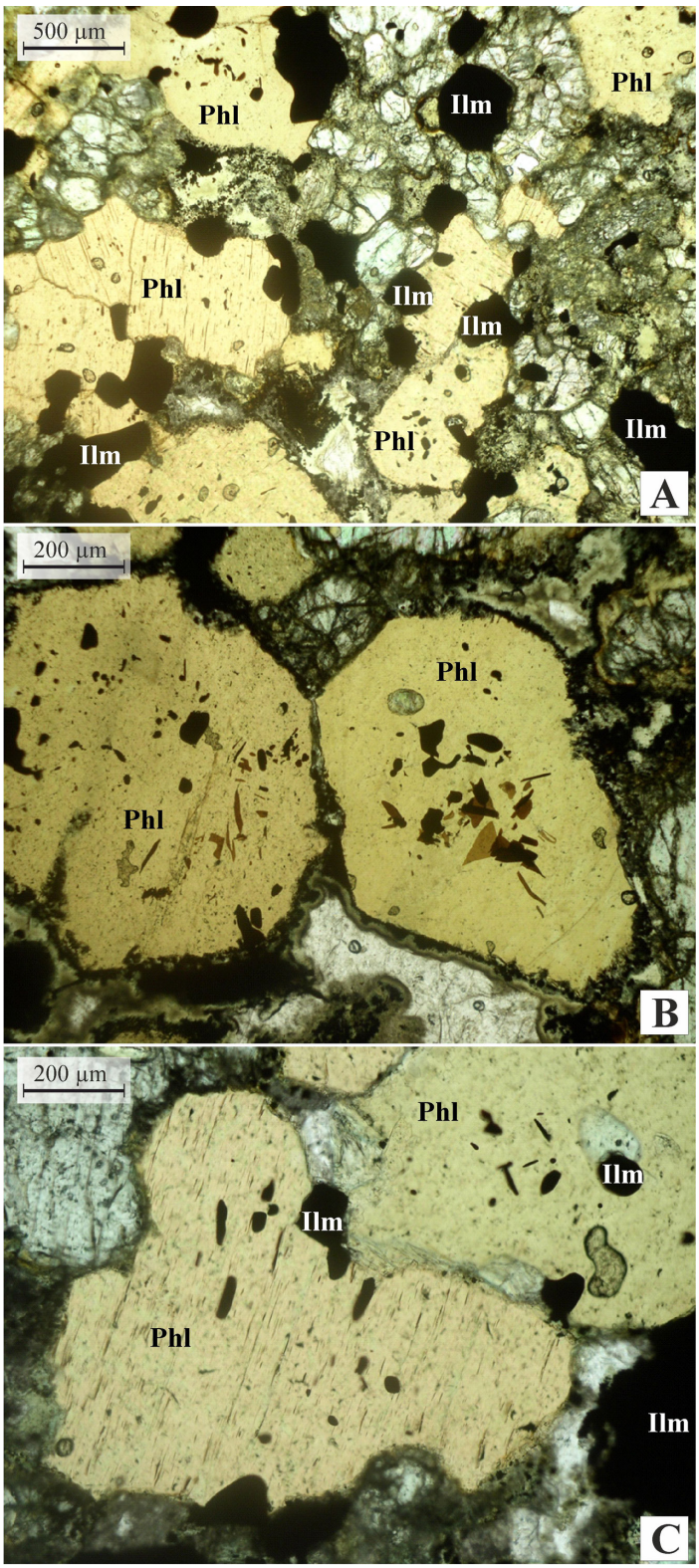


**Fig. 17.** The photomicrographs of thin section. Porphyrous phlogopite plates in the garnetless Phl-Ilm websterite.

*A* – the matrix contains small prismatic grains of pyroxenes (mainly orthopyroxene) and oval grains of ilmenite. *B* and *C* –regular plates of phlogopite. Thin transparent lamellae of ilmenite are located along cleavage in mice (*B*). Larger elongated and isometric grains of ilmenite with oval-shaped boundaries tend to be located at the marginal zones of the mica plates (*A, B*). Images without an analyzer.

**Рис. 17.** Порфировидная структура в безгранатовом Phl-Ilm вебстерите.

*A* – в породе присутствуют мелкие призматические зерна пироксенов (преимущественно ортопироксен) и овальные, изометричные зерна ильменита. *B* и *C* – правильные вкрапленники флогопита. По спайности в слюде располагаются тонкие просвечивающие пластинки ильменита (*B*). Более крупные удлиненные и изометричные зерна ильменита с овальными ограничениями тяготеют к краевым зонам пластинок слюды (*A, B*). Фото шл. без анализатора.

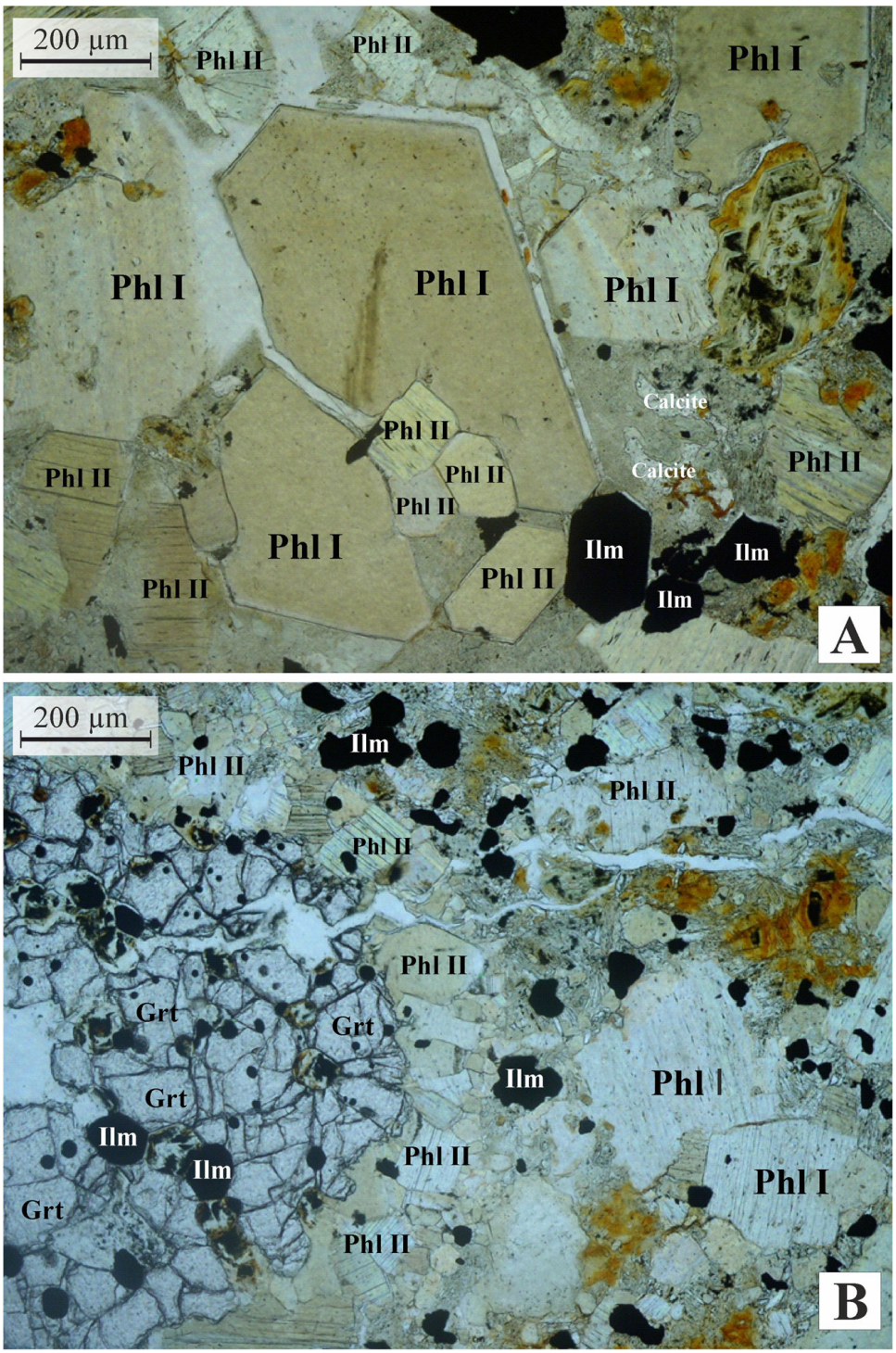


**Fig. 18.** The photomicrographs of thin section. Porphyrous texture in the Phl-Ilm olivine websterite.

*A* – regularly-faceted plates of Phl I, flakes of Phl II and an ideally faceted grain of ilmenite are visible. Late serpentine and carbonate are developed in the rock matrix. (*B*) The grain of strongly resorbed garnet that is surrounded by the Phl II reaction rim. In garnet numerous roundish grains of ilmenite are relics of replacing during garnetization. Garnet possibly was caught of the residual high-potassium melt from the earlier intrusive phase. In the rock matrix, irregular grains of ilmenite are resorbed with later processes, including serpentization and carbonitization. Images without an analyzer.

**Рис. 18.** Порфировидная структура в Phl-Ilm оливиновом вебстерите.

*A* – видны правильно ограненные вкрапленники Phl I, пластинки флогопита II (Phl II) и идеально ограненный вкрапленник ильменита. В матрице породы развиты поздние серпентин и карбонат. *B* – «вкрапленник» сильно резорбированного граната, окруженного реакционной каймой из Phl II. В гранате видны многочисленные округлые зерна ильменита, являющиеся реликтами замещения при гранатизации. По-видимому, гранат попал в остаточный высоко-калиевый расплав из более ранней интрузивной фазы. Неправильные зерна ильменита в матрице резорбированы более поздними процессами (серпентинизация, карбонатизация). Фото шл. без анализатора.

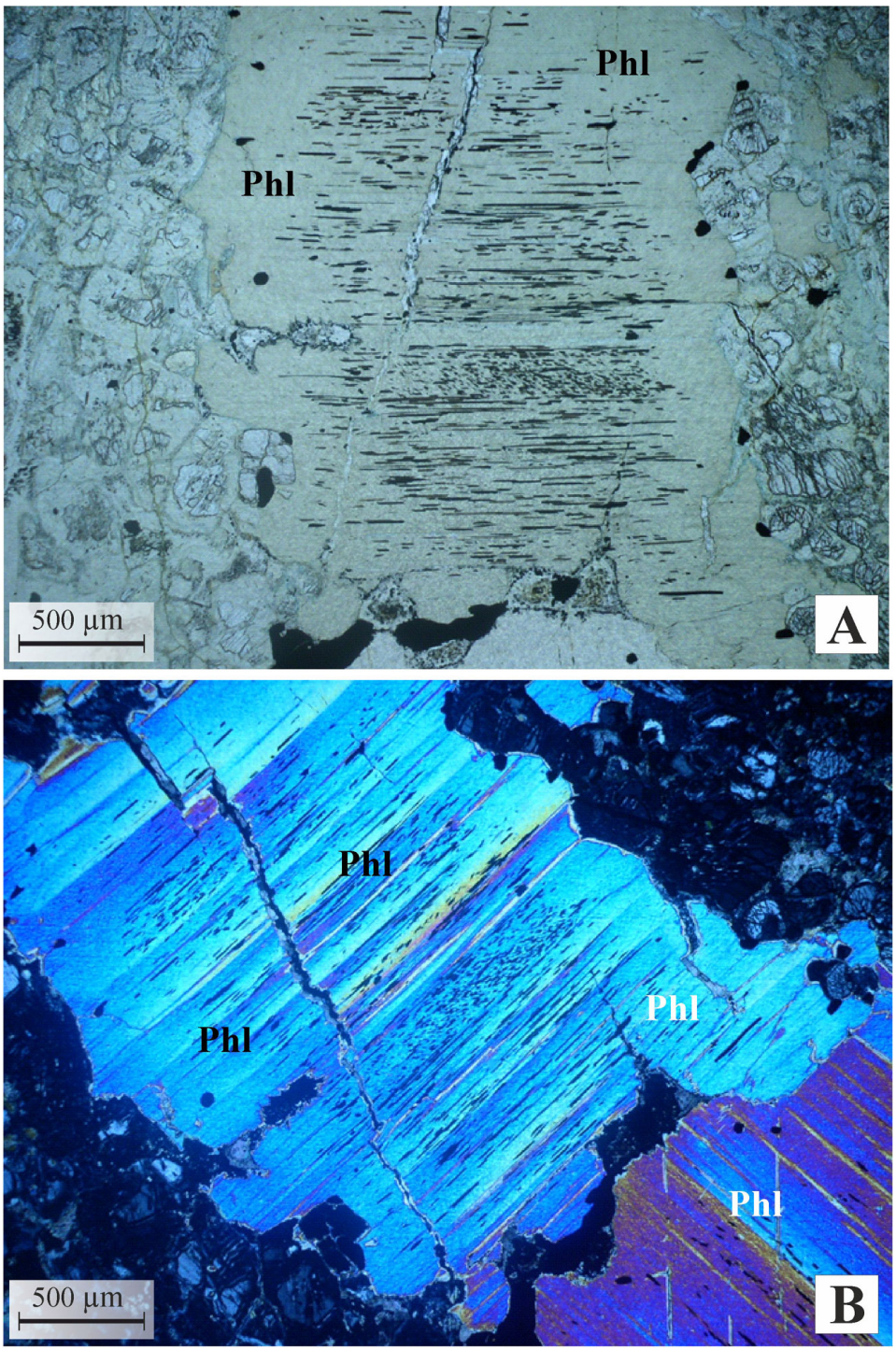


**Fig. 19.** The photomicrographs of thin section. Oriented thin lamllae of ilmenite in porphyrous phlogopite.

Larger oval-shaped ilmenite grains tend to be located at the margins of the phlogopite plates. Images: *A* – without an analyzer; *B* – in crossed nicols.

**Рис. 19.** Ориентированное положение тонких пластинок ильменита в порфировидных вкрапленниках флогопита.

К краям вкрапленников тяготеют более крупные овальные зерна ильменита. Фото шл.: *A* – без анализатора, *B* – в × николях.

corresponds to the development of the deformation zones which led to the formation of specific deformed phlogopite-amphibole parageneses with titanian chromite and resorbed relics of clinopyroxene and ilmenite. It is most probable than these rocks developed on the rocks of the Phl-Ilm series in the root parts of the deep fault zones.

Representative compositions of minerals from two

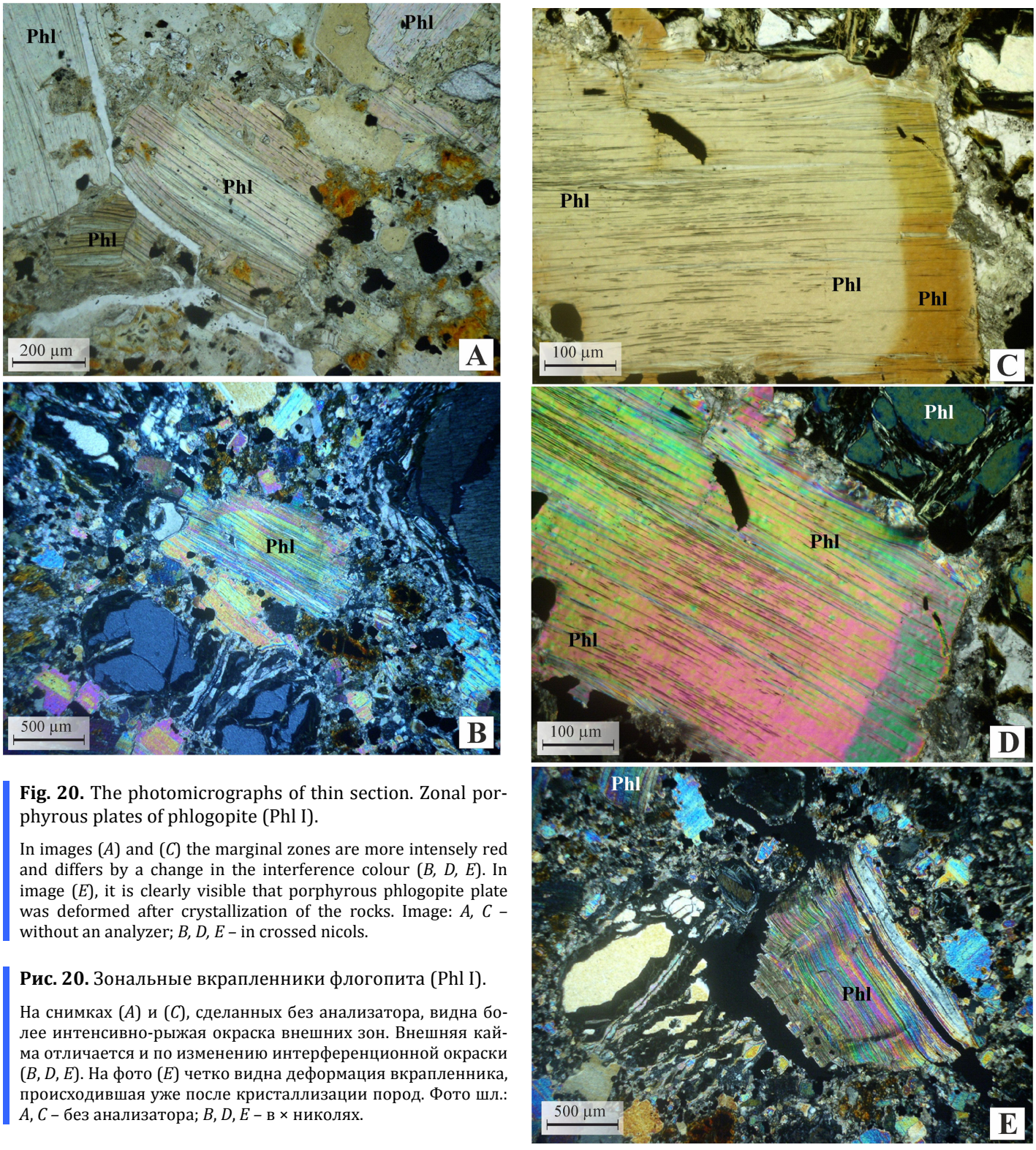


**Fig. 20.** The photomicrographs of thin section. Zonal porphyrous plates of phlogopite (Phl I).

In images (*A*) and (*C*) the marginal zones are more intensely red and differs by a change in the interference colour (*B, D, E*). In image (*E*), it is clearly visible that porphyrous phlogopite plate was deformed after crystallization of the rocks. Image: *A, C* – without an analyzer; *B, D, E* – in crossed nicols.

**Рис. 20.** Зональные вкрапленники флогопита (Phl I).

На снимках (*A*) и (*C*), сделанных без анализатора, видна более интенсивно-рыжая окраска внешних зон. Внешняя кайма отличается и по изменению интерференционной окраски (*B*, *D*, *E*). На фото (*E*) четко видна деформация вкрапленника, происходившая уже после кристаллизации пород. Фото шл.: *A*, *C* – без анализатора; *B*, *D*, *E* – в × николях.

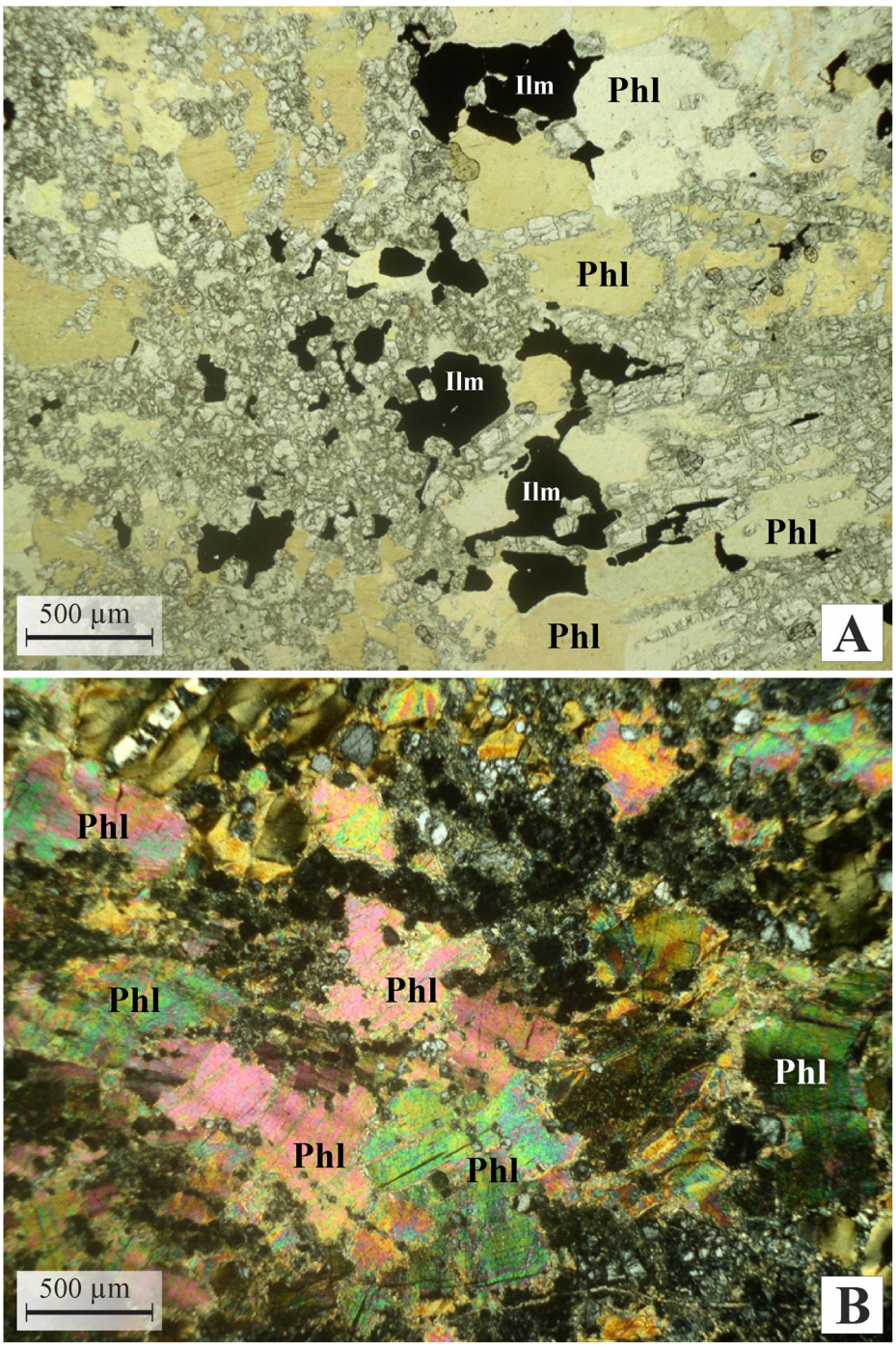


**Fig. 21.** The photomicrographs of thin section. General texture of the deformed phlogopite-amphibole rocks.

The ragged edges of the phlogopite plates and ilmenite grains are visible. The rocks also contain elongated partially bended crystals of monoclinal amphibole. Images: *A* without an analyzer; *B* – in crossed nicols.

**Рис. 21.** Общий вид структуры в деформированных флогопит-амфиболовых породах.

Видны совершенно неправильные, с «оборванными» краями пластинки флогопита и зерна ильменита с изъеденными, зазубренными контурами. Остальное выполнение породы состоит из удлиненных частично изогнутых кристаллов моноклинного амфибола. Фото шл.: *A* – без анализатора; *B* – в × николях.

xenoliths of the Mg series with metasomatic phlogopite and amphibole and five xenoliths of the Phl-Ilm series of hyperbasites are given in Table. The main rock-forming minerals in the metasomatically altered xenoliths of the Mg series are not significantly different from the corresponding minerals from xenoliths that do not contain any metasomatic minerals [*Solov'eva et al., 1994*]. This observation may indirectly suggest that

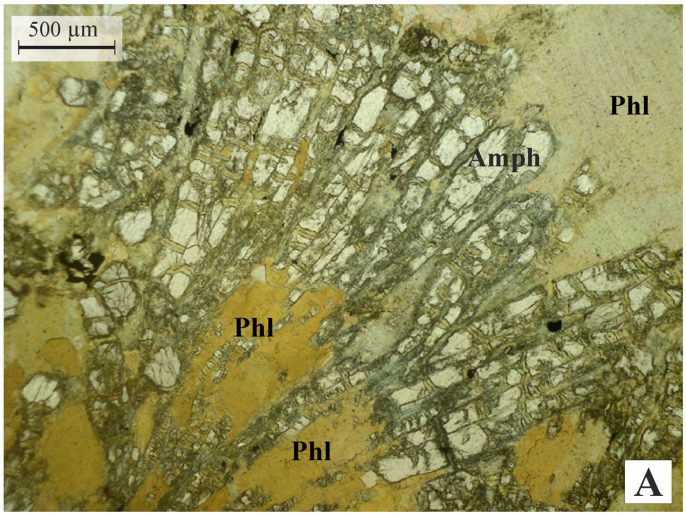


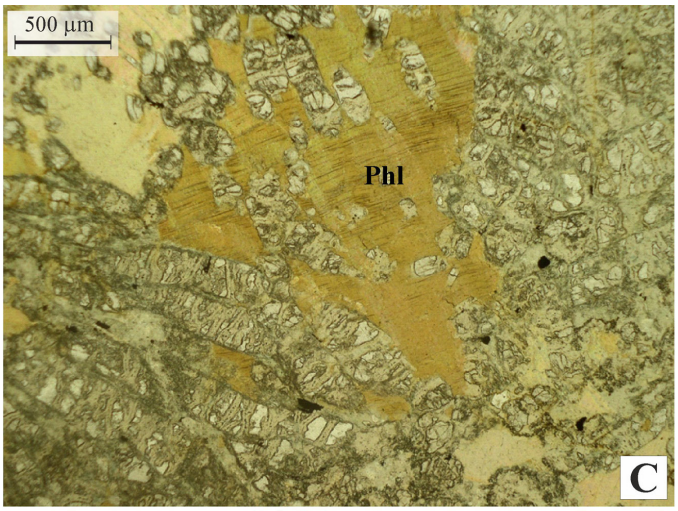


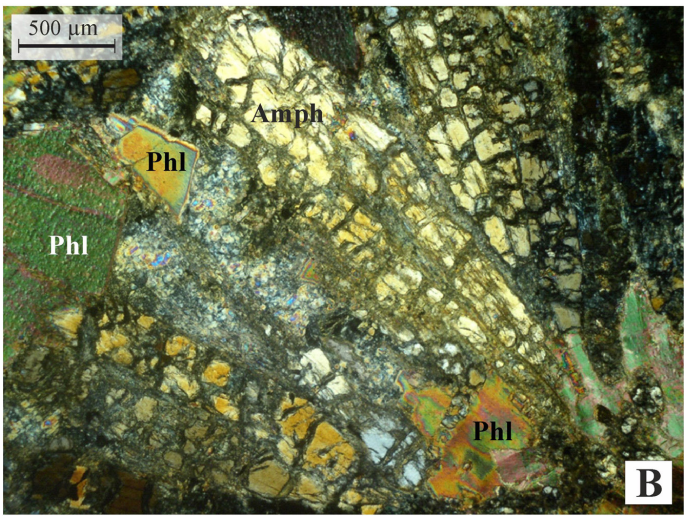


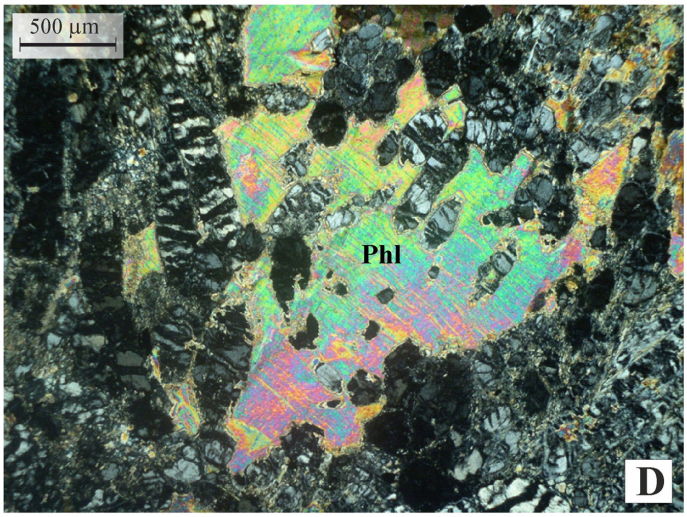


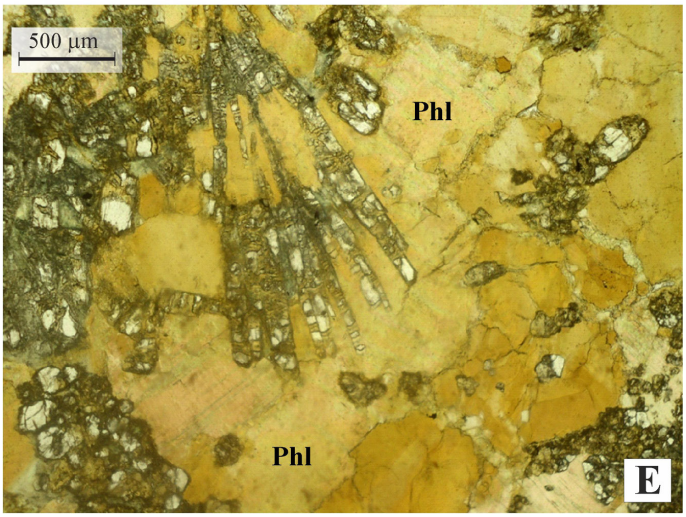


**Fig. 22.** The photomicrographs of thin section. Monoclinal amphibole rosettes in intergrowths with irregular-shaped grains of phlogopite (*A*–*E*).

Images (*C*) and (*D*) show a typical torch-like form of phlogopite, bended cleavage of mica and elongated crystals of amphibole. (*E*) The initially single phlogopite plate was granulated into several small platelets. Images: *A, C, E* – without an analyzer; *B, D* – in crossed nicols.

**Рис. 22.** Розетки моноклинного амфибола в срастках с неправильными зернами флогопита (*A*–*E*).

На снимках (*C*) и (*D*) видна характерная факелообразная форма флогопита, а также изгиб спайности слюды и удлиненных кристаллов амфибола. *E* – изначально единая пластинка флогопита гранулирована на несколько более мелких. Фото шл.: *A, C, E* – без анализатора; *B, D* – в × николях.

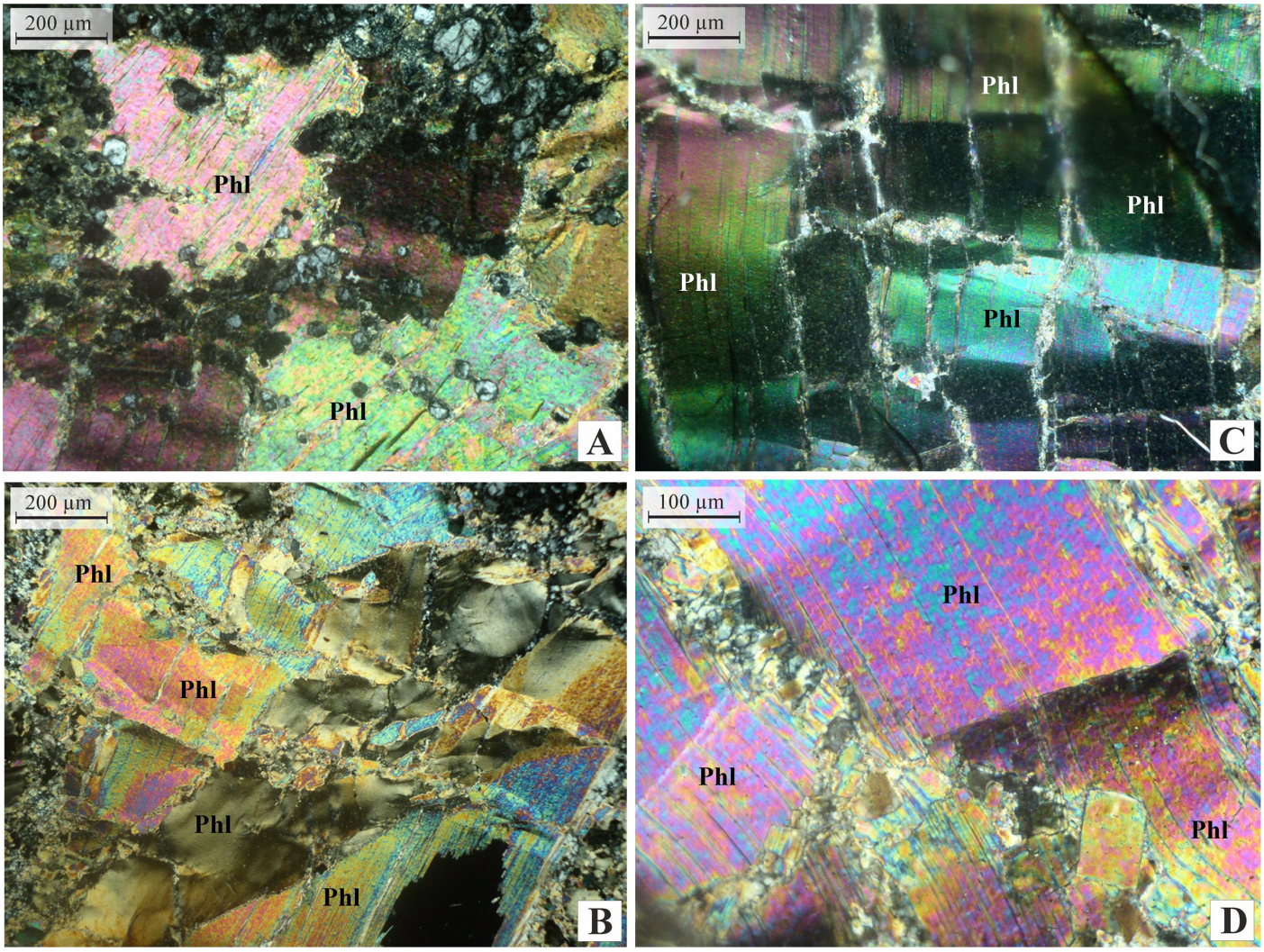


**Fig. 23.** The photomicrographs of thin section. Deformation of phlogopite plates.

*A* – general view of the plates in the rock. Images (*B, C, D*) show that the phlogopite plates were granulated into blocks of various orientations, which are separated by the fine-grained mica aggregate. The latter contains a few larger regular-shaped recrystallized platelets. Images in crossed nicols.

**Рис. 23.** Характер деформации пластинок флогопита.

*A* – общий вид пластинок в породе. При более сильном увеличении видно (*B, C, D*), как пластинки слюды гранулируются на разноориентированные блоки, разделенные мелкочешуйчатым слюдяным агрегатом. В последнем появляются более крупные правильные перекристаллизованные пластинки Фото шл. в × николях.

the entire magnesian pyroxenite-peridotite series was subject to metasomatic modification, and the process took place with chemical reequilibration of primary and newly-formed minerals. This assumption is supported by the lack of zonation in the crystals of phlogopite and amphibole. Unlike the corresponding minerals in the Phl-Ilm series of hyperbasites, the main minerals in the Mg series are characterized by the higher magnesium index (Mg#), considerably lower contents of $TiO_2$, FeO and higher contents of $Cr_2O_3$ (Table).

In diagrams Mg# – $TiO_2$ and Mg# – $Cr_2O_3$, metasomatic phlogopite points from rocks of the Mg series are significantly distant from the field of points of mica from the phlogopite-ilmenite parageneses (Fig. 24, *A*, *B*). The metasomatic phlogopite from rocks of the Mg series contains more chrome oxide, less titanium oxide and have significantly higher contents of magnesium. Within the parageneses of the Phl-Ilm series, the lowest magnesium contents and the highest titanium contents are typical of mica from the deformed phlogopite-amphibole rocks. The phlogopite flakes from these rocks have either high or low contents of chrome. In the more intensively coloured marginal rims of the phlogopite plates, especially in the large porphyrious ones, the Mg content is lower, while the content of

**Chemical compositions of minerals in deep-seated xenoliths with phlogopite and phlogopite-amphibole mineralization in the Obnazhennaya kimberlitic pipe**

**Химический состав минералов в глубинных ксенолитах с флогопитовой и флогопит-амфиболовой минерализацией в кимберлитовой трубке Обнаженная**

| Sample | 74-817 | | | | | | 74-296a | | | 7-365 | | |
|---|---|---|---|---|---|---|---|---|---|---|---|---|
| Mineral | Ol | Opx | Cpx | Grt | Phl | Amph | Opx | Phl | Amph | Ol | Opx | Cpx |
| $SiO_2$ | 40.39 | 57.06 | 54.16 | 41.97 | 39.31 | 47.28 | 57.24 | 39.06 | 46.97 | 39.83 | 56.02 | 54.72 |
| $TiO_2$ | | 0.04 | 0.19 | 0.08 | 0.46 | 0.59 | 0.04 | 0.50 | 0.42 | | 0.19 | 0.35 |
| $Al_2O_3$ | | 0.93 | 3.57 | 22.72 | 14.89 | 9.79 | 1.34 | 15.05 | 10.83 | 0.04 | 1.24 | 2.67 |
| $Cr_2O_3$ | | 0.14 | 0.89 | 1.21 | 0.69 | 0.59 | 0.34 | 0.90 | 1.81 | 0.02 | 0.22 | 0.78 |
| FeO | 7.38 | 4.54 | 2.71 | 8.23 | 3.14 | 3.32 | 5.25 | 3.00 | 3.56 | 14.58 | 8.88 | 5.16 |
| MnO | 0.06 | 0.05 | 0.08 | 0.31 | 0.04 | 0.04 | 0.11 | 0.02 | 0.08 | 0.14 | 0.14 | 0.12 |
| MgO | 51.32 | 36.75 | 15.41 | 21.59 | 25.31 | 20.44 | 36.08 | 25.20 | 20.23 | 45.90 | 32.32 | 16.22 |
| CaO | | 0.22 | 19.97 | 4.21 | | 8.91 | | | 8.71 | 0.04 | 0.82 | 18.32 |
| $Na_2O$ | | 0.05 | 3.06 | 0.02 | 1.09 | 5.34 | | 2.00 | 5.10 | | 0.227 | 2.42 |
| $K_2O$ | | | | | 9.52 | 1.21 | | 6.63 | 0.37 | | 0.020 | 0.01 |
| NiO | 0.45 | 0.14 | | | 0.12 | 0.05 | 0.02 | 0.18 | 0.08 | 0.26 | | |
| SrO | | | | | | | | 0.16 | | | | |
| BaO | | | | 0.06 | 0.76 | 0.04 | | 2.78 | | | | |
| F | | 0.11 | 0.05 | 0.10 | 0.06 | 0.07 | | | | | | |
| Cl | | | | | 0.03 | 0.03 | | | | | | |
| **Total** | **99.73** | **100.02** | **100.07** | **100.47** | **95.38** | **97.65** | **100.42** | **92.70** | **98.16** | **100.80** | **100.08** | **100.78** |
| Mg# | 92.52 | 93.50 | 91.02 | 82.37 | 93.48 | 91.65 | 92.4 | 93.7 | 91.0 | 84.9 | 86.6 | 84.9 |

| Sample | 7-365 | | | | | O-42-87 | | | O-22-87 | | | |
|---|---|---|---|---|---|---|---|---|---|---|---|---|
| Mineral | Grt | Phl I | Phl II | Ilm I | Ilm II | Cpx | Phl | Ilm | Opx | Cpx | Phl | Ilm |
| $SiO_2$ | 41.57 | 39.93 | 39.70 | 0.00 | 0.04 | 54.26 | 40.94 | 0.03 | 55.602 | 54.60 | 42.06 | 0.00 |
| $TiO_2$ | 0.64 | 1.88 | 2.82 | 51.06 | 42.16 | 0.16 | 0.90 | 50.48 | 0.05 | 0.31 | 1.24 | 50.09 |
| $Al_2O_3$ | 20.79 | 12.83 | 12.77 | 0.88 | 0.66 | 0.96 | 11.53 | 0.08 | 0.095 | 0.94 | 11.29 | 0.11 |
| $Cr_2O_3$ | 1.35 | 0.47 | 0.51 | 2.30 | 2.06 | 0.67 | 0.09 | 0.87 | 0.063 | 0.56 | 0.13 | 0.83 |
| FeO | 12.12 | 6.14 | 6.29 | 33.37 | 44.15 | 5.32 | 6.07 | 38.20 | 9.671 | 5.45 | 6.04 | 39.02 |
| MnO | 0.41 | 0.03 | 0.02 | 0.18 | 0.65 | 0.11 | 0.02 | 0.35 | 0.237 | 0.13 | 0.01 | 0.35 |
| MgO | 17.88 | 22.53 | 21.34 | 11.80 | 5.96 | 15.82 | 24.96 | 10.05 | 34.053 | 16.11 | 24.83 | 9.74 |
| CaO | 5.03 | | | 0.04 | 0.25 | 20.10 | | 0.01 | 0.36 | 20.15 | | 0.02 |
| $Na_2O$ | 0.09 | 0.21 | 0.31 | | | 2.496 | 0.23 | | 0.105 | 2.17 | 0.27 | |
| $K_2O$ | 0.01 | 10.47 | 10.46 | | | 0.01 | 10.58 | | | | 10.55 | |
| NiO | | | | | | | | | | | | |
| SrO | | | 0.032 | | | | | | | | 0.002 | |
| BaO | | | 0.352 | | | | 0.131 | | | | 0.134 | |
| F | | 0.162 | 0.268 | | | | 0.332 | | | | 0.418 | |
| Cl | | 0.048 | | | | | 0.011 | | | | | |
| **Total** | **99.89** | **94.68** | **94.86** | **99.58** | **95.93** | **99.90** | **95.78** | **100.08** | **100.24** | **100.40** | **96.98** | **100.16** |
| Mg# | 72.4 | 86.7 | 85.8 | 38.6 | 19.4 | 84.1 | 88.0 | 31.9 | 86.2 | 84.1 | 88.0 | 30.8 |

| Sample | 7-371 | | | | | |
|---|---|---|---|---|---|---|
| Mineral | Ol | Phlc | Phlr | Phlr1 | Ilm | Amph |
| $SiO_2$ | 38.37 | 39.99 | 39.46 | 38.79 | 0.07 | 55.93 |
| $TiO_2$ | 0.00 | 1.01 | 3.02 | 4.02 | 52.77 | 0.16 |
| $Al_2O_3$ | 0.00 | 13.07 | 13.17 | 13.26 | 0.68 | 1.06 |
| $Cr_2O_3$ | 0.00 | 0.49 | 1.12 | 0.58 | 1.83 | 0.37 |
| FeO | 20.42 | 5.86 | 6.04 | 5.91 | 32.24 | 2.41 |
| MnO | 0.18 | 0.01 | 0.02 | 0.04 | 0.25 | 0.05 |
| MgO | 41.78 | 22.67 | 22.05 | 21.46 | 11.97 | 22.60 |
| CaO | 0.05 | | | | 0.03 | 6.73 |
| $Na_2O$ | | 0.80 | 0.37 | 0.32 | | 5.56 |
| $K_2O$ | | 9.65 | 9.40 | 10.47 | | 3.14 |
| NiO | 0.072 | | | | | |
| SrO | | 0.015 | 0.023 | | | 0.03 |
| BaO | | 0.129 | 0.064 | 0.065 | | 0.05 |

End of Table

Окончание таблицы

| Sample | 7-371 | | | | | |
|---|---|---|---|---|---|---|
| **Mineral** | **Ol** | **Phlc** | **Phlr** | **Phlr1** | **Ilm** | **Amph** |
| **F** | | 0.321 | 0.173 | 0.236 | | 0.33 |
| **Cl** | | 0.015 | 0.013 | 0.016 | | |
| **Total** | **100.87** | **94.02** | **94.93** | **95.14** | **99.84** | **98.41** |
| **Mg#** | 78.5 | 87.3 | 86.7 | 86.6 | 39.8 | 94.3 |

Note. Mg series: sample **74-817** – Grt olivine websterite with Phl-Amph metasomatic veinlets; sample **74-296a** – megacrystalline Grt orthopyroxenite with metasomatic Phl–Amph mineralization. Series of Phl-Ilm hyperbasites: sample **7-365** – Phl-Ilm garnetized lherzolite; sample **O-42/87** – porphirous Phl-Ilm websterite; sample **O-22/87** – porphirous Phl-Ilm olivine websterite; sample **7-371** – deformed Phl-Amph rocks with accessory Ti-chromite and relict Ilm.

Примечание. Mg серия: обр. **74-817** – Grt оливиновый вебстерит с метасоматическими прожилками Phl и Amph; обр. **74-296a** – мегакристаллический Grt ортопироксенит с метасоматической Phl – Amph минерализацией. Серия Phl-Ilm гипербазитов: обр. **7-365** – Phl-Ilm гранатизированный лерцолит; обр. **O-42/87** – порфировидный Phl-Ilm вебстерит; обр. **O-22/87** – порфировидный Phl-Ilm оливиновый вебстерит; обр. **7-371** – деформированная Phl-Amph порода с акцессорным Ti-хромитом и с реликтовым Ilm.

titanium is higher as compared to those in the central parts (Fig. 24). A possible cause might be that exsolution textures of ilmenite precipitated in the centre of phlogopite grains, and this process was accompanied by depletion by titanium oxide and ferrum oxide. At the margins of the large phlogopite plates, ilmenite exsolution lamellae are lacking and changed by larger isometric grains. This suggests that the main portion of ilmenite precipitated from the melt at the latest stages of crystallization simultaneously with the growth of the late rims on phlogopite and of small mica flakes of the second generation.

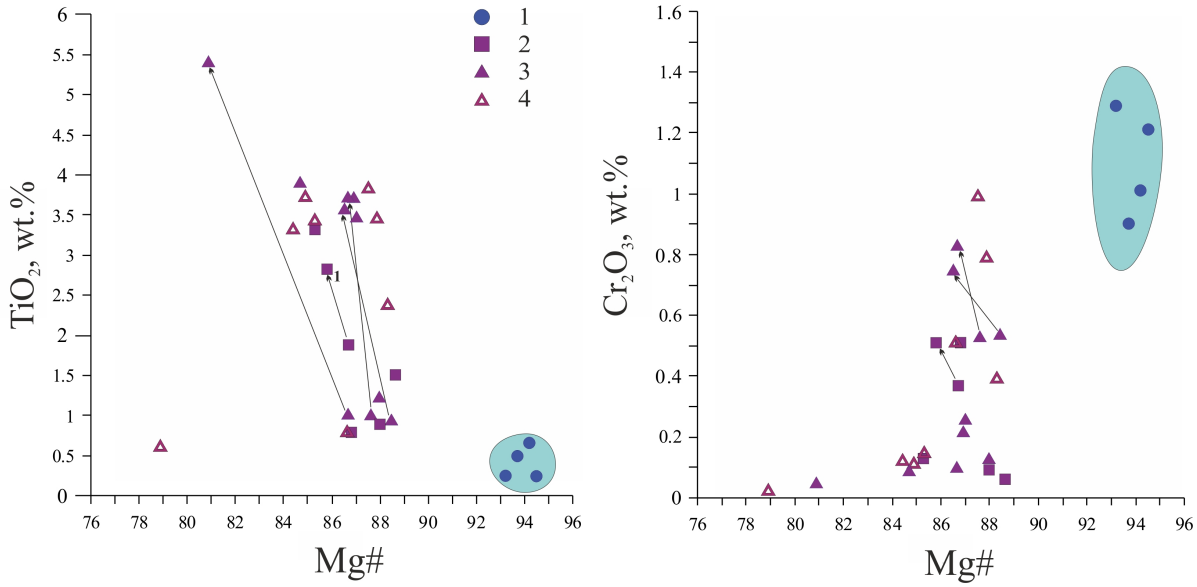


**Fig. 24.** Mg# vs. $TiO_2$ and Mg# vs. $Cr_2O_3$ in phlogopites from rocks of the Mg pyroxenite-peridotite and Phl-Ilm series.

*1* – metasomatic phlogopite from the rocks of the Mg series; *2* – phlogopite from garnetless and garnetized Phl-Ilm hyperbasites; *3* – phlogopite from porphyrous garnetless Phl-Ilm hyperbasites; *4* – phlogopite from deformed phlogopite-amphibole rocks with newly-formed chromite. Arrow tips refer to compositions of phlogopite from the marginal zones of porphyrous plates or from smaller platelets in the matrix (solid symbols).

**Рис. 24.** Соотношение Mg# - $TiO_2$ и Mg# - $Cr_2O_3$ во флогопите из пород Mg пироксенит-перидотитовой и Phl-Ilm серий.

*1* – метасоматический флогопит из пород Mg серии; *2* – флогопит из безгранатовых и гранатовых Phl-Ilm гипербазитов; *3* – флогопит из порфировидных безгранатовых Phl-Ilm гипербазитов; *4* – флогопит из деформированных флогопит-амфиболовых пород с новообразованным хромитом и реликтовыми ильменитом, клинопироксеном. Окончание стрелок означает состав флогопита из краевых зон порфировидных выделений флогопита или из мелких пластинок в матрице (залитые значки).

By its chemical composition, amphibole represented by typical pargasite in the Phl-Amph metasomatites of the Mg series (Table) [*Ukhanov et al*., *1988*]) is obviously different from K-richterite from the deformed phlogopite-amphibole rocks. The latter has significantly larger contents of $SiO_2$ and $K_2O$ and several-fold lower contents of $Cr_2O_3$ and $Al_2O_3$.

Ilmenites from the Phl-Ilm parageneses of all the three groups have high contents of MgO (9.7–12 %), except the late micrograin in the cavern in the garnet grain (6 %). All the ilmenites listed in Table 1 differ from ilmenites of the ultrabasic diamond paragenesis with the lower content of $TiO_2$ [*Patrin et al*., *2004*]. The micrograin from the cavern in the garnet grain contains more MnO and less $TiO_2$ as compared to other analysed ilmenites. Considering the content of the main oxides, the relict resorbed ilmenite from the deformed phlogopite-amphibole rocks (7-371) is similar to Ilm I from the garnetized Phl-Ilm lherzolite (7-365). Ilmenite from garnetless Phl-Ilm websterites (O-42/87 and O-22/87) contains significantly less $Cr_2O_3$ and more FeO as compared to ilmenite from the garnetized Phl-Ilm lherzolite (7-365). Due to high contents of phlogopite and ilmenite and higher contents of Fe in silicates, the Phl-Ilm hyperbasites from the pipes of the Kuoika field belong to high-potassium, titanian and ferrous basites-ultrabasites.

## 4. $^{40}Ar/^{39}Ar$ DATING OF MICA

Results of $^{40}Ar/^{39}Ar$ dating for mica from the phlogopite-containing xenoliths of the Mg pyroxenite-peridotite and Phl-Ilm series are given in Fig. 25. According to the $^{40}Ar/^{39}Ar$ method, ages of phlogopites from the metasomatic inclusions and veins in the garnet olivine websterite (74-817) range from ~1640 to 1800 Ma. Mica from the garnetless Phl-Ilm parageneses (O-22/87 and O-42/87) has similar ages for high-temperature stages (~869 and 851 Ma, respectively) (Fig. 25). Phlogopite from the garnetized Phl-Ilm lherzolites (12/7 and 7-365) has significantly younger ages, ~608 and 495 Ma, respectively. Mica from the deformed phlogopite-amphibole rocks Sl-3 has an approximate age of 167 Ma, which is close to the age of kimberlites of the Kuoika field [*Howarth et al.*, *2014*].

## 5. DISCUSSION AND RESULTS

The age determinations for mica confirm the conclusion based on the data on petrography, mineralogy and chemistry of the minerals: the phlogopite and phlogopite-amphibole parageneses of the Mg pyroxenite-peridotite and the Phl-Ilm basite-ultrabasite series are represented by two discrete mantle rock associations in the mantle lithosphere of the Birekte terrain. Xenoliths with the combined presence of minerals of both series are lacking.

The specific features, such as the cumulative type of banding, high temperatures (1250–1500 °C) of the start of crystallization of exsolution megacrystals of pyroxenes, the presence of deformed globules of sulphides and others, give grounds to consider the Mg pyroxenite-peridotite series as the layered intrusion in the mantle [*Ukhanov et al., 1988; Solov'eva et al., 1994*]. The average chemical composition of the rocks in this series is close to that of the Al-undepleted komatiites [*Solov'eva et al., 1994*]. For four crystals of zircon from kimberlites of the Rubin pipe (Kuoika filed), ages determined by the SHRIMP method fall into two groups, 1.8–2.1 (~1.95 Ga in average) and 2.3–2.6 Ga (~2.4 Ga in average) [*Nasdala et al*., *2014*]. In the opinion of the authors, the above-mentioned ranges reflect the main evolution stages of the crust in the Birekte block. The average most ancient age (~2.4 Ga) is actually similar to the formation time of the Birekte terrain (~2.4 Ga), according to [*Rosen*, *2003*]. In the first approximation, this age can be viewed as the formation time of the layered magmatic Mg series in the mantle. The average age of 1.9 Ga corresponds, according to [*Rosen*, *2003*], to the accretion time of the Birekte terrain to the Siberian craton (~1.8–1.9 Ga). The estimated $^{40}Ar/^{39}Ar$ age of metasomatic phlogopite from the xenolith in the Mg series (~1.64–1.8 Ga) is close to the latest event. The lower age of mica may be due to a partial loss of $^{40}Ar$. The rocks of the Mg series from the Obnazhennaya pipe have another particular feature: values of $\delta^{18}O$ in garnets and clinopyroxenes from peridotites, websterites and garnet clinopyroxenites have a considerable admixture of subduction oxygen (Fig. 26 [*Taylor et al*., *2003, 2005*]). It can thus be assumed that at some stage, the mantle lithosphere substance under the Birekte block was subject to fluid-melt metasomatism in the subduction zone. According to [*Pernet-Fisher et al*., *2015*], radiogenic osmium was supplied into the mantle lithosphere of the Birekte block by sulphur-rich fluids from the subduction zone between 1.7 and 2.2 Ga, and this period correlates with the age of phlogopite from the phlogopite-amphibole metasomatites (1.64–1.8 Ga). As noted in the petrographic description, the phlogopite-amphibole veinlets have a typical magmatic euhedral texture, i.e. they might have crystallised from the melts. Based on the reviewed data, it can be suggested that in the mantle lithosphere of the Birekte terrain, phlogopite-amphibole metasomatism of the rocks of the magnesian pyroxenite-peridotite series was resulted by fluids-melts ascending from the subduction zone.

This assumption does not contradict to the data on the mantle pyroxenites containing graphite and the lower-crust metabasite granulites from the kimberlitic

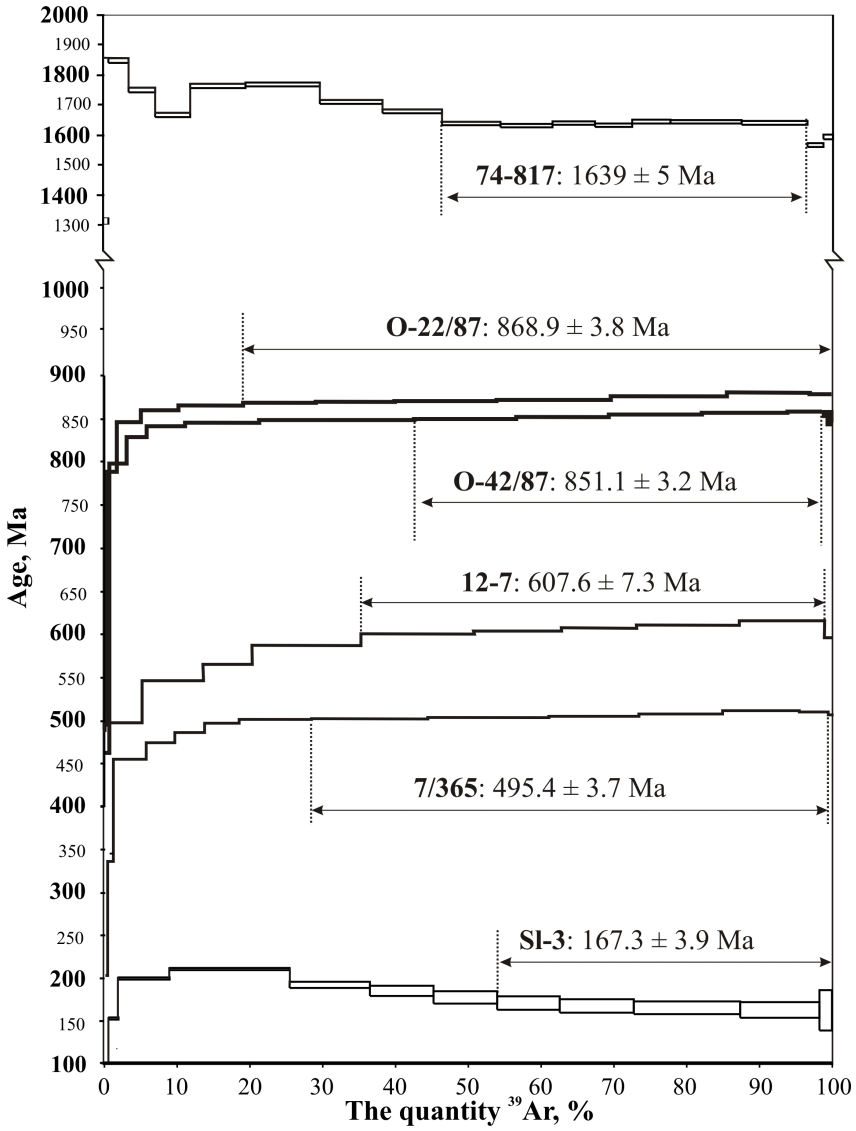


**Fig. 25.** Ages of phlogopite (according to the $^{40}Ar/^{39}Ar$ method) in xenoliths of the Mg pyroxenite-peridotite series (sample 74-817) and the Phl- Ilm series (sample O-22/87 and O-42/87 – garnetless Phl-Ilm hyperbasites; 12-7 and 7-365 – intensive garnetized Phl-Ilm lherzolites; sample Sl-3 – deformed Phl-Amph rock). Mineral compositions of samples 74-817, O-22/87, O-42/87 and 7-365 are given in Table.

**Рис. 25.** Возраст флогопитов, полученный методом $^{40}Ar/^{39}Ar$ датирования в ксенолитах Mg пироксенит-перидотитовой серии (обр. 74-817) и Phl- Ilm серии (обр. O-22/87, O-42/87 – безгранатовые Phl-Ilm гипербазиты; 12-7 и 7-365 – интенсивно гранатизированные Phl-Ilm лерцолиты; обр. Сл-3 – деформированная Phl-Amph порода). Состав минералов из образцов 74-817, O-22/87, O-42/87, 7-365 приведен в таблице.

pipes of the Kuoika field. In the deep-seated xenoliths from the Obnazhennaya and Slyudyanka kimberlitic pipes, graphite-bearing orthopyroxenites and websterites are found, which are viewed as crystal cumulative rocks in boninite dykes with the biogenic matter added under island-arc conditions, as suggested by studies of oxygen and sulphur isotopes and bulk rock geochemistry [*Solov'eva et al., 2010*]. By their geochemical characteristics, the xenoliths of basite granulites from the pipes of the Kuoika field (which are representing the lower crust in the Birekte terrain) are determined as result of fractional crystallization of the island-arc low-potassium tholeiites [*Solov'eva et al., 2004*]. Therefore, it can be assumed that the accretion of the Birekte microcontinent/terrain to the Siberian craton, being a larger continental block, took place about 1.8 Ga ago in the subduction zone.

The Phl–Ilm parageneses of the xenoliths represent the differentiated magmatic series with ubiquitous processes of subsolidus garnetization and autometasomatic phlogopitization. According to results of the whole-rock chemical analyses, the rocks of this series

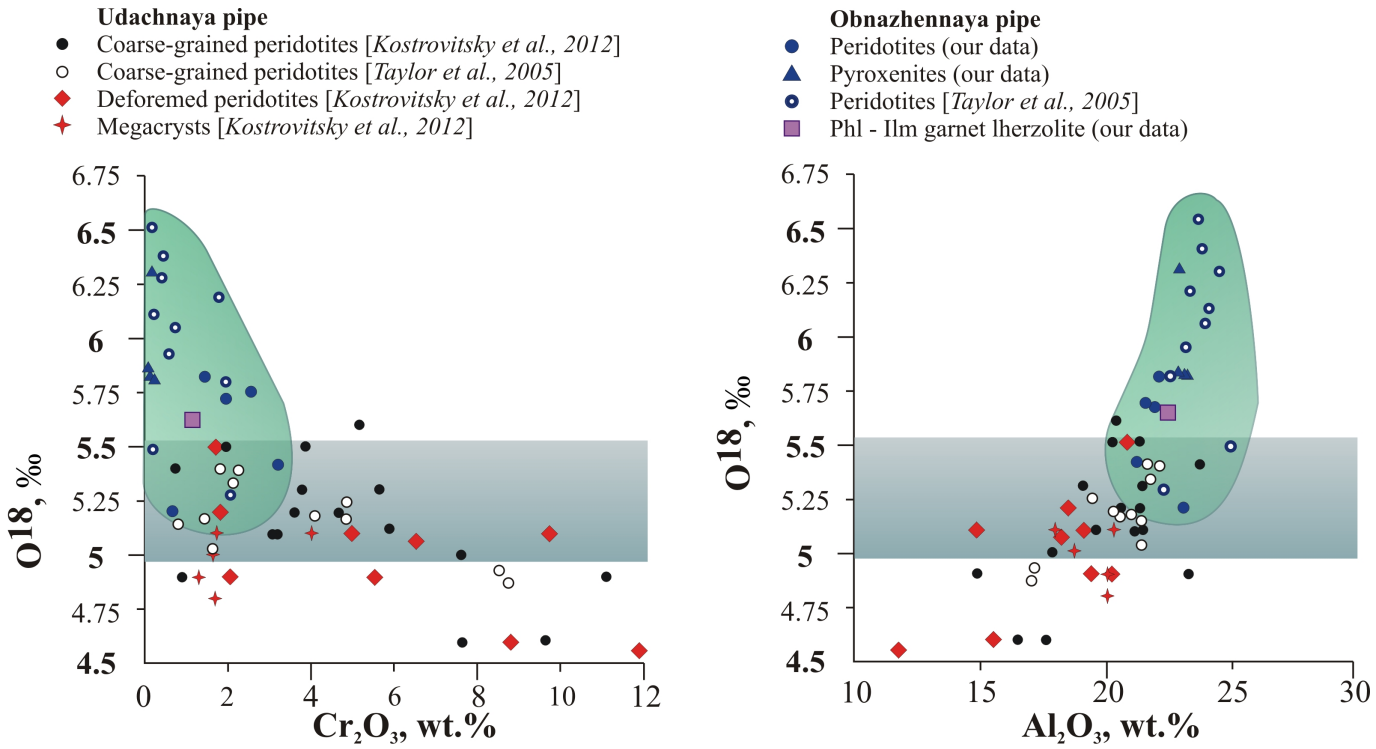


**Fig. 26.** $Cr_2O_3$ vs. $^{18}O$ and $Al_2O_3$ vs. $^{18}O$ in garnet from peridotites and pyroxenites of the Mg series, from Phl-Ilm lherzolite (Obnazhennaya pipe) and coarse-grained and deformed peridotites and megacrysts (Udachnaya pipe). The range of mantle values for garnet is shown by the blue strip.

**Рис. 26.** Соотношение $Cr_2O_3$ – $^{18}O$ и $Al_2O_3$ – $^{18}O$ в гранате из перидотитов и пироксенитов Mg серии, из Phl-Ilm лерцолита (трубка Обнаженная) и из зернистых, деформированных перидотитов и мегакристов трубки Удачная. Голубая полоса – диапазон мантийных значений для граната.

can be classified as high-potassium basites and ultrabasites. The most ancient ages of phlogopites in this series (869 and 851 Ma) belong to the Upper Proterozoic and are close to the early age of the alkali-ultrabasic carbonatite Tomtor pluton-volcano (800 Ma, [*Entin et al., 1990*]). The younger ages of phlogopite in the garnetized parageneses (608 and 495 Ma, samples 12-7 and 7/365) may be related to the loss of radiogenic $^{40}Ar$ due to its substitution by garnet. During this process, $H_2O$, K, Ba, F and Cl were supplied into the upper layers of the crust and mantle. The age of phlogopite in xenolith Sl-307 (167 Ma), which is close to the age of the kimberlites of the Kuoika field, may reflect the influence of the kimberlitic melt.

In this context, the entire complex series of the Phl-Ilm parageneses from the xenoliths in kimberlites of the Kuoika field can be considered as the high-potassium mantle rocks being deep sources of high-potassium magmatites on the surface. The latter may include the complex long-term alkali ultrabasic-carbonatite Tomtor pluton-volcano as well as the series of dykes and sub-effusive K-basites and lamproites [*Shpunt, Shamshina, 1989*; *Kiselev et al., 2012*]. Besides, it is not improbable that the intensively deformed phlogopite-amphibole rocks, that mark the deep weakened zones in the mantle lithosphere, guided the alkali potassium magma to the surface. According to [*Li et al., 2008*], the formation of Rodinia to its maximum size took place between 1000 and 900 Ma, and the first major episode of its breakup due to the plume impact occurred 825 Ma ago. Although the ages of phlogopite from the Phl-Ilm websterites (869 and 851 Ma) are by 45, 25 Ma larger than the initial stage of Rodinia breakup according to [*Li et al., 2008*], it can be assumed that the formation of the high-potassium, titanian and ferrous magmatites in the mantle took place in advance of their occurrence on the surface. In the Siberian craton, the Rodinia breakup was accompanied by magmatism due to the impact of the Upper Proterozoic plume [*Li et al., 2008*].

Thus, the Phl-Amph metasomatites developed in the mantle lithosphere of the Birekte block on the rocks of the early magmatic Mg pyroxenite-peridotite series are markers of the stage related to the accretion of this block to the Siberian craton (~1.8–1.9 Ga). In the mantle lithosphere of the Birekte terrain, the magmatic series of the Phl-Ilm hyperbasites occurred much later (~869–851 Ma) corresponding to the start of Rodinia

breakup [*Li et al*., *2008*]. The deformed phlogopite-amphibole rocks were formed as metasomatites of the deep fault zones drained the upper mantle.

## 6. Main conclusions

1. The petrographic, chemical and geochemical features of discussed phlogopite and phlogopite-amphibole xenoliths from the kimberlitic pipes of the Kuoika field (i.e. the north-eastern part of the Siberian craton) are evidence of different stages in the evolution of the mantle lithosphere of the Birekte terrain.

2. The Phl-Amph metasomatites develop on the rocks of the complex Mg pyroxenite-peridotite series of the xenoliths, belonging to the ancient layered mantle intrusion. In the rocks of this series, the Phl-Amph metasomatism gave geochemical features of the subduction zone and marked the stage related to the accretion of the Birekte continental block to the Siberian craton (~1.8–1.9 Ga).

3. The complex series of the Phl-Ilm rocks taken out by kimberlites of the Kuoika field in the form of xenoliths is the later series as compared to the Mg pyroxenite-peridotite series and the Phl-Amph metasomatites. The Phl-Ilm hyperbasites can be classified as typical mantle potassium ultrabasic-basic magmatites. The deformed phlogopite-amphibole rocks are typical metasomatic rocks of the deep faults; they formed at the expense of the earlier Phl-Ilm rocks. The outset of the formation of the magmatic series of the Phl-Ilm hyperbasites in the mantle lithosphere of the Birekte terrain (~869–851 Ma) corresponds to the start of Rodinia breakup [*Li et al*., *2008*]. The high-potassium, titanian and ferrous rocks of this series were the feeding mantle sources for potassium ultrabasic and basic magmatism in the Upper Proterozoic and the Lower Cambrian in the northern part of the Siberian platform.

## 7. References

*Entin A.R., Zaitsev A.I., Nenashev N.I., Vasilenko V.B., Orlov A.I., Tyan O.A., Olkhovik Yu.A., Olshtynsky S.I., Tolstov A.V.*, 1990. About the sequence of geological events related to the intrusion of the Tomtor alkaline ultramafic and carbonatite massif, North-Western Yakutia. *Geologiya i Geofizika* (*Russian Geology and Geophysics*) 31 (12), 42–50 (in Russian) [*Энтин А.Р., Зайцев А.И., Ненашев Н.И., Василенко В.Б., Орлов А.И., Тян О.А., Ольховик Ю.А., Ольштынский С.И., Толстов А.В.* О последовательности геологических событий, связанных с внедрением Томторского массива ультраосновных щелочных пород и карбонатитов (Северо-Западная Якутия) // *Геология и геофизика*. 1990. Т. 31. № 12. С. 42–50].

*Garanin V.K., Kudryavtseva G.P., Khar'kiv A.D., Chistyakova V.F.*, 1985. The mineralogy of ilmenite hyperbasites from the Obnazhennaya kimberlitic pipe. *Izvestiya AN SSSR*, *Seriya geologicheskaya* (5), 85–101 (in Russian) [*Гаранин В.К., Кудрявцева Г.П., Харькив А.Д., Чистякова В.Ф.* Минералогия ильменитовых гипербазитов из кимберлитовой трубки Обнаженная // *Известия АН СССР, серия геологическая*. 1985. № 5. С. 85–101].

*Howarth G.H., Barry P.H., Pernet–Fisher J.F., Baziotis I.P., Pokhilenko N.P., Pokhilenko L.N., Bodnar R.J., Taylor L.A., Agashev A.M.*, 2014. Superplume metasomatism: Evidence from Siberian mantle xenoliths. *Lithos* 184–187, 209–224. http://dx.doi.org/10.1016/j.lithos.2013.09.006.

*Ignatiev A.V., Velivetskaya T.A.*, 2004. The laser method of sample-preparation for analyses of stable isotopes of oxygen in silicates and oxides. In: Abstracts of the XVII Stable Isotopes Symposium. Institute of Geochemistry and Analytical Chemistry, Moscow, p. 96–97 (in Russian) [*Игнатьев А.В., Веливецкая Т.А.* Лазерная методика подготовки проб для анализа стабильных изотопов кислорода силикатов и окислов // XVII симпозиум по стабильным изотопам: Тезисы докладов. М.: ГЕОХИ, 2004. С. 96–97].

*Khar'kiv A.D., Zinchuk N.N., Kryuchkov A.I.,* 1998. Primary Diamond Deposits of the World. Nedra Publishing House, Moscow, 555 p. (in Russian) [*Харькив А.А., Зинчук Н.Н., Крючков А.И.* Коренные месторождения алмазов мира. М.: Недра, 1998. 555 с.].

*Kiselev A.I., Yarmolyuk V.V., Kolodeznikov I.I., Struchkov K.K., Egorov K.N.*, 2012. The northeastern boundary of the Siberian craton and its formation peculiarities (derived from occurrences of Early Cambrian and Devonian intraplate magmatism). *Doklady Earth Sciences* 447 (1), 1252–1258. http://dx.doi.org/10.1134/S1028334X12110098.

*Kostrovitsky S.I., Solov'eva L.V., Gornova M.A., Alymova N.V., Yakovlev D.A., Ignat'ev A.V., Velivetskaya T.A., Suvorova L.F.*, 2012. Oxygen isotope composition in minerals of mantle parageneses from Yakutian kimberlites. *Doklady Earth Sciences* 444 (1), 579–584. http://dx.doi.org/10.1134/S1028334X12050030.

*Li Z.X., Bogdanova S.V., Collins A.S., Davidson A., De Waele D., Ernst R.E., Fitzsimons I.C.W., Fuck R.A., Gladkochub D.P., Jacobs J., Karlstrom K.E., Lu S., Natapov L.M., Pease V., Pisarevsky S.A., Thrane K., Vernikovsky V.*, 2008. Assembly, configuration, and break-up history of Rodinia: a synthesis. *Precambrian Research* 160 (1–2), 179–210. http://dx.doi.org/10.1016/j.precamres.2007.04.021.

*Menzies M.A., Hawkesworth C.J.* (Eds.), 1987. Mantle Metasomatism. Academic Press, New York, 472 p.

*Nasdala L., Kostrovitsky S.I., Kennedy A.K., Zeug M., Esenkulova S.A.*, 2014. Retention of radiation damage in zircon xenocrysts from kimberlites, Northern Yakutia. *Lithos* 206–207, 252–261. http://dx.doi.org/10.1016/j.lithos.2014.08.005.

*Parfenov L.M., Kuzmin M.I.* (Eds.), 2001. Tectonics, Geodynamics and Metallogeny of the Sakha Republic (Yakutia). MAIK Nauka/Interperiodika, Moscow, 571 p. (in Russian) [*Тектоника, геодинамика и металлогения территории Республики Саха* (*Якутия*) / Отв. ред. Л.М. Парфенов, М.И. Кузьмин. М.: МАИК «Наука/Интерпериодика», 2001. 571 с.].

*Patrin G.S., Matsuk S.S., Kostrovitsky S.I., Alymova N.V.*, 2004. The mineralogical features and chemistry of ilmenite from lower mantle xenoliths. *Mineralogical Journal* (Ukraine) 26 (4), 60–77 (in Russian) [*Патрин Г.С., Мацюк С.С., Костровицкий С.И., Алымова Н.В.* Минералогия ильменита из глубинных ксенолитов в кимберлитах (типохимизм, генетическое и поисковое значение) // *Мінералогічний журнал* (Украина). 2004. Т. 26. № 4. С. 60–77].

*Pernet-Fisher J.F., Howarth G.H., Pearson D.G., Woodland S., Barry P.H., Pokhilenko N.P., Pokhilenko L.N., Agashev A.M., Taylor L.A.*, 2015. Plume impingement on the Siberian SCLM: Evidence from Re-Os isotope systematics. *Lithos* 218–219, 141–154. http://dx.doi.org/10.1016/j.lithos.2015.01.010.

*Pokhilenko N.P., Sobolev N.V., Kuligin S.S., Shimizu N.*, 1999. Peculiarities of distribution of pyroxenite paragenesis garnets in Yakutian kimberlites and some aspects of the evolution of the Siberian craton lithospheric mantle. In: Proceedings of the 7th International Kimberlite Conference. RedRoof Design, Cape Town, p. 689–698.

*Rosen O.M.*, 2003. The Siberian craton: tectonic zonation and stages of evolution. *Geotectonics* 37 (3), 175–192.

*Shpunt B.R., Shamshina E.A.*, 1989. The Late Vendian potassium alkaline volcanites of the Olenek uplift (North-Eastern Siberian platform). *Doklady AN SSSR* 307 (2), 678–682 (in Russian) [*Шпунт Б.Р., Шамшина Э.А.* Поздневендские калиевые щелочные вулканиты Оленекского поднятия (северо-восток Сибирской платформы) // *Доклады АН СССР*. 1989. Т. 307. № 2. С. 678–682].

*Solovieva L.V., Egorov K.N., Markova M.E., Kharkiv A.D., Popolitov K.E., Barankevich V.G.*, 1997. Mantle metasomatism and melting in deep-seated xenoliths from the Udachnaya pipe, their possible relationship with diamond and kimberlite formation. *Geologiya i Geofizika* (*Russian Geology and Geophysics*) 38 (1), 172–193.

*Solov'eva L.V., Gornova M.A., Markova M.E., Lozhkin V.I.*, 2004. Geochemical identification of granulites in xenoliths from Yakutian kimberlites. *Geochemistry International* 42 (3), 220–235.

*Solov'eva L.V., Vladimirov B.M., Dneprovskaya L.V., Maslovskaya M.N., Brandt S.B.*, 1994. Kimberlite and Kimberlite-Similar Rocks: Material of the Upper Mantle beneath Ancient Platforms. Nauka, Novosibirsk, 256 p. (in Russian) [*Соловьева Л.В., Владимиров Б.М., Днепровская Л.В., Масловская М.Н., Брандт С.Б.* Кимберлиты и кимберлитоподобные породы: вещество верхней мантии под древними платформами. Новосибирск: Наука, 1994. 256 с.].

*Solov'eva L.V., Yasnygina T.A., Kostrovitsky S.I.*, 2010. Isotopic and geochemical evidence for a subduction setting during formation of the mantle lithosphere in the northeastern part of the Siberian craton. *Doklady Earth Sciences* 432 (2), 799–803. http://dx.doi.org/10.1134/S1028334X1006019X.

*Taylor L.A., Snyder G.A., Keller R., Remley D.A., Anand M., Wiesli R., Valley J., Sobolev N.V.*, 2003. Petrogenesis of group A eclogites and websterites: Evidence from the Obnazhennaya kimberlite, Yakutia. *Contributions to Mineralogy and Petrology* 145 (4), 424–443. http://dx.doi.org/10.1007/s00410-003-0465-y.

*Taylor L.A., Spetsius Z.V., Wiesli R., Spicuzza M., Valley J.W.*, 2005. Diamondiferous peridotites from oceanic protoliths: Crustal signatures from Yakutian kimberlites. *Russian Geology and Geophysics* (*Geologiya i Geofizika*) 46 (12), 1176–1184.

*Travin A.V., Yudin D.S., Vladimirov A.G., Khromykh S.V., Volkova N.I., Mekhonoshin A.S., Kolotilina T.B.*, 2009. Thermochronology of the Chernorud granulite zone, Ol'khon region, Western Baikal area. *Geochemistry International* 47 (11), 1107–1124. http://dx.doi.org/10.1134/S0016702909110068.

*Ukhanov A.V., Ryabchikov I.D., Khar'kiv A.D.*, 1988. Lithospheric Mantle of Yakutian Kimberlite Province. Nauka, Moscow, 286 p. (in Russian) [*Уханов А.В., Рябчиков И.Д., Харькив А.Д.* Литосферная мантия Якутской кимберлитовой провинции. М.: Наука, 1988. 286 с.]

**Solov'eva, Lidia V.,** Doctor of Geology and Mineralogy, Lead Researcher
Institute of the Earth's Crust, Siberian Branch of RAS
128 Lermontov street, Irkutsk 664033, Russia
Tel.: (3952)425434; ✉ e-mail: Solv777@crust.irk.ru

**Соловьева Лидия Васильевна,** докт. геол.-мин. наук, в.н.с.
Институт земной коры СО РАН
664033, Иркутск, ул. Лермонтова, 128, Россия
Тел.: (3952)425434; ✉ e-mail: Solv777@crust.irk.ru

**Kalashnikova, Tatiana V.,** Junior Researcher
A.P. Vinogradov Institute of Geochemistry, Siberian Branch of RAS
1A Favorsky street, Irkutsk 664033, Russia
e-mail: Kalashnikova@igc.irk.ru

**Калашникова Татьяна Владимировна,** м.н.с.
Институт геохимии им. А.П. Виноградова СО РАН
664033, Иркутск, ул. Фаворского, 1А, Россия
e-mail: Kalashnikova@igc.irk.ru

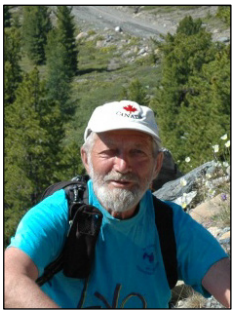

**Kostrovitsky, Sergei I.,** Doctor of Geology and Mineralogy, Lead Researcher
A.P. Vinogradov Institute of Geochemistry, Siberian Branch of RAS
1A Favorsky street, Irkutsk 664033, Russia
e-mail: Serkost@igc.irk.ru

**Костровицкий Сергей Иванович,** докт. геол.-мин. наук, в.н.с.
Институт геохимии им. А.П. Виноградова СО РАН
664033, Иркутск, ул. Фаворского, 1А, Россия
e-mail: Serkost@igc.irk.ru

**Ivanov, Alexei V.,** Doctor of Geology and Mineralogy, Lead Researcher
Institute of the Earth's Crust, Siberian Branch of RAS
128 Lermontov street, Irkutsk 664033, Russia
Tel.: 8(3952)427117; e-mail: aivanov@crust.irk.ru

**Иванов Алексей Викторович,** докт. геол.-мин. наук, в.н.с.
Институт земной коры СО РАН
664033, Иркутск, ул. Лермонтова, 128, Россия
Тел.: 8(3952)427117; e-mail: aivanov@crust.irk.ru

**Matsuk, Stanislav S.,** Doctor of Geology and Mineralogy, Lead Researcher
M.P. Semenenko Institute of Geochemistry, Mineralogy and Ore Formation
of the National Academy of Sciences of Ukraine
34 Acad. Palladin Ave., Kyiv 03680, Ukraine
e-mail: Smatsyuk@hotmail.com

**Мацюк Станислав Степанович,** докт. геол.-мин. наук, в.н.с.
Институт геохимии, минералогии и рудообразования им. Н.П. Семененко НАН Украины
03680, Киев, проспект Акад. Палладина, 34, Украина
e-mail: Smatsyuk@hotmail.com

**Suvorova, Ludmila F.,** Candidate of Chemistry, Chief Specialist
A.P. Vinogradov Institute of Geochemistry, Siberian Branch of RAS
1A Favorsky street, Irkutsk 664033, Russia
e-mail: Suvorova@igc.irk.ru

**Суворова Людмила Филипповна,** канд. хим. наук, главный специалист
Институт геохимии им. А.П. Виноградова СО РАН
664033, Иркутск, ул. Фаворского, 1А, Россия
e-mail: Suvorova@igc.irk.ru